

1 **Revisiting the variation of the climate feedback parameter and its**
2 **connection to ocean enthalpy uptake**

3 Diego Jiménez-de-la-Cuesta*

4 *Max-Planck-Institut für Meteorologie, Hamburg, Deutschland*

5 *Corresponding author: Diego Jiménez-de-la-Cuesta, diego.jimenez@mpimet.mpg.de

ABSTRACT

6 Models indicate a time-varying radiative response of the Earth system to CO₂ forcing (Andrews
7 et al. 2012; Zhou et al. 2016). This variation implies a significant uncertainty in the estimates of
8 climate sensitivity to increasing atmospheric CO₂ concentration (Hawkins and Sutton 2009; Grose
9 et al. 2018). In energy-balance models, the temporal variation is represented as an additional
10 feedback mechanism (Winton et al. 2010; Geoffroy et al. 2013a; Rohrschneider et al. 2019),
11 which also depends on the ocean temperature change. Models and observations also indicate
12 that a spatio-temporal pattern in surface warming controls this additional contribution to the
13 radiative response (Ceppi and Gregory 2017; Zhou et al. 2016). Some authors picture the effect
14 as a purely atmosphere-based feedback change (Stevens et al. 2016), reducing the role of the
15 ocean's enthalpy-uptake variations. For the first time, I derive, using a widely-known linearised
16 conceptual energy-balance model (Winton et al. 2010; Geoffroy et al. 2013a; Rohrschneider et al.
17 2019), an explicit mathematical expression of the radiative response and its temporal evolution.
18 This expression connects the spatio-temporal warming pattern to an effective thermal capacity,
19 stemming from changes in the ocean enthalpy uptake. In comparison with more realistic energy-
20 balance frameworks, and unlike the notion of additional feedback mechanisms, I show that an
21 expanded effective thermal capacity better explains the variation of the radiative response, naturally
22 connects with the spatio-temporal surface warming pattern, and provides a non-circular framework
23 to explain the variation of the climate feedback parameter.

24 *Significance statement.* Understanding the factors that change the Earth’s radiative response
25 to CO₂ forcing is central to reduce the uncertainty in the climate sensitivity estimates. The
26 current atmospheric-only view on the problem of the time-varying climate feedback parameter
27 unnecessarily hides the ocean’s role. This work shows a novel perspective for the problem,
28 enabling the development of a more general theory.

29 **1. Introduction**

30 Climate models show a wide range of temporal variation in their radiative response to CO₂ forcing
31 (Senior and Mitchell 2000; Andrews et al. 2012; Ceppi and Gregory 2017). This variation appears
32 in numerical experiments where the atmospheric CO₂ concentration is raised and maintained
33 constant afterwards. The rise in the atmospheric CO₂ concentration modifies the Earth’s emissivity
34 to longwave radiation, resulting in surface warming. Surface warming modifies the radiative flux at
35 the top of the atmosphere (TOA). The modified flux tends to cancel the energy imbalance introduced
36 by the radiative forcing. Surface warming also changes other variables, such as the atmospheric
37 temperature and humidity, that further modify the radiative flux. These changes are the feedback
38 mechanisms on surface warming. The net rate at which the globally-averaged surface warming
39 reduces the globally-averaged TOA imbalance is known as the climate feedback parameter.

40 If the feedback mechanisms did not change with time, the climate feedback parameter would be
41 constant, and a diagram of globally-averaged TOA imbalance change versus surface temperature
42 change (*NT*-diagram) would be linear. However, climate models present *NT*-diagrams with
43 different degrees of curvature, indicating a non-constant climate feedback parameter (Andrews
44 et al. 2012; Ceppi and Gregory 2017) (presented schematically on figure 1). The degree of
45 curvature is also modified by forcing strength (Senior and Mitchell 2000; Meraner et al. 2013;
46 Rohrschneider et al. 2019). Hence, the variation of the climate feedback parameter comes from

47 temporal and state dependencies. Observations indicate that a spatio-temporal pattern of surface
48 warming modifies cloud feedback in decadal timescales by altering atmospheric stability, leading
49 to feedback changes that depend not only on surface warming (Zhou et al. 2016; Mauritsen 2016).
50 The spatio-temporal warming pattern is modified by forcing, leading to both the temporal and the
51 state dependency.

52 In a globally-averaged energy-balance framework, the energy imbalance change at the TOA, N ,
53 is equal to the forcing F plus the radiative response of the system R , $N = F + R$. Following the
54 classical picture of the linearised feedback mechanisms depending only on the surface warming
55 (Gregory et al. 2002) T_u , we should have $R \sim \lambda T_u$, where λ is a constant climate feedback parameter.
56 Thus, if we consider a constant forcing F , the slope of the NT -diagram would be constant and
57 equal to λ , in contradiction with observations and complex models as discussed above. Thus,
58 either the non-linear component plays a more significant role, or the feedback mechanisms depend
59 on more than the surface warming.

60 This problem is not resolved if we consider the structure of the system as two coupled layers
61 of different thermal capacities: the atmosphere + land + upper ocean layer or upper layer, and
62 the deep ocean or deep layer (Winton et al. 2010; Geoffroy et al. 2013b; Rohrschneider et al.
63 2019). The timescales provided by the two thermal capacities and the layers' coupling only provide
64 a longer equilibration period and do not alter the climate feedback parameter. The upper-layer
65 budget including a deep-ocean enthalpy uptake term is $N_u = F + \lambda T_u - H$. The deep-layer budget
66 is equal to the deep-ocean enthalpy uptake: $N_d = H$. Thus, the energy imbalance at the TOA is
67 $N = N_u + N_d = F + \lambda T_u$. Therefore, the radiative response is identical to the classical approach.

68 If we reflect on the dichotomy of the constant λ and the varying slope seen in complex models, we
69 should note that the constant λ is a reference value of the climate feedback parameter. This reference
70 value is associated with the linear approximation of the radiative response R in the neighbourhood

71 of the initial state. In the same manner, the deep-ocean enthalpy uptake H represents a reference
72 value around the initial state (Winton et al. 2010; Geoffroy et al. 2013a). The difference between
73 the transient and the reference H dynamically enlarges the deep-ocean thermal capacity (Geoffroy
74 et al. 2013b), providing a effective deep-ocean thermal capacity. As this effective thermal capacity
75 affects the flux between the upper and deep layers, it will also modify the surface temperature,
76 connecting the notion of a spatio-temporal warming pattern with changes in the ocean’s energy
77 content.

78 Geoffroy et al. (2013a) introduced a perturbed deep-ocean enthalpy uptake in the upper-layer
79 budget, $H' := \varepsilon H$, where ε is the efficacy parameter. The efficacy parameter represents the effect
80 of the spatio-temporal warming pattern on the effective deep-ocean energy uptake. The deep-layer
81 budget is still equal to H , leading to a different energy imbalance at the TOA: $N = F + \lambda T_u + (H - H')$.
82 The $H - H'$ term seems to break the energy conservation principle. Instead, it suggests some new
83 deep-ocean-driven ”feedback mechanisms” or, as discussed before, an expanded effective thermal
84 capacity. Held et al. (2010); Geoffroy et al. (2013a) briefly showed the point of view of the
85 thermal capacity. However, the focus of their studies did not allow further exploration along this
86 path. Others (e.g. Armour et al. 2013; Stevens et al. 2016) explicitly favour the deep-ocean-driven
87 ”feedback mechanisms”, deeming the oceanic point-of-view as artificial. Choosing the ”feedback”
88 interpretation, however, presents the $H - H'$ term as an *ad-hoc* modification, leaving undefined the
89 origin of the spatio-temporal warming pattern, and obscuring the relationship with the feedback
90 mechanisms.

91 Considering the analytical solutions of the modified two-layer model, I derive for the first time
92 an explicit mathematical expression for the slope of the NT -diagrams, including the explicit time
93 evolution of this slope. At its core, this expression has the ratio of change of the energy stored
94 by the upper and deep layers. Its physical interpretation shifts the attention from the deep-ocean-

95 driven "feedback mechanisms" to the atmosphere-ocean coupling in the variation of the climate
 96 feedback parameter. The interpretation of these results is that the atmosphere-ocean coupling sets
 97 the spatio-temporal warming pattern. Afterwards, the atmosphere adjusts, leading to the changes
 98 in the feedback mechanisms.

99 2. Theory

100 The following equations define the modified linearised two-layer model (Geoffroy et al. 2013a)

$$101 \quad \begin{cases} C_u \dot{T}_u = F + \lambda T_u - \varepsilon \gamma (T_u - T_d) \\ 102 \quad C_d \dot{T}_d = \gamma (T_u - T_d) \end{cases}$$

103 where the first equation corresponds to the upper-layer budget and the second equation to the deep
 104 layer. The constant λ and γ are the climate feedback parameter and the rate of deep-ocean enthalpy
 105 uptake in the neighbourhood of the initial state. C_u and C_d are respectively the thermal capacities
 106 (per unit area) of the upper and deep layers. T_u and T_d are temperature anomalies referred to the
 107 initial state and the dotted quantities are time total derivatives. The planetary imbalance is the sum
 108 of both equations, resulting in $N = F + \lambda T_u + (1 - \varepsilon)\gamma(T_u - T_d)$. Nonetheless, it is better to write
 109 these equations in the following fashion

$$110 \quad \begin{cases} \dot{T}_u = F' + \lambda' T_u - \varepsilon \gamma' (T_u - T_d) \\ 111 \quad \dot{T}_d = \gamma'_d (T_u - T_d) \end{cases} \quad (1)$$

112 where $F' := F/C_u$ with units of Ks^{-1} and, $\lambda' := \lambda/C_u$, $\gamma' := \gamma/C_u$ and $\gamma'_d := \gamma/C_d$ with units of
 113 s^{-1} . Equations (1) are a system of linear ordinary differential equations (Geoffroy et al. 2013a;
 114 Rohrschneider et al. 2019). Although the solutions are standard and widely discussed in other
 115 articles (e.g. Geoffroy et al. 2013a; Rohrschneider et al. 2019), their analyses are not sufficient
 116 for my purpose. In the following, I proceed by summarising the relevant facts, leaving the full
 117 mathematical discussion to the appendix of this article.

118 The homogeneous ($F' \equiv 0$) version of the system (1) has two distinct eigenvalues $\mu_{\pm} := (\hat{\lambda} \pm \kappa)/2$,
 119 where $\hat{\lambda} := \lambda' - \varepsilon\gamma' - \gamma'_d$ and $\kappa^2 := \hat{\lambda}^2 + 4\lambda'\gamma'_d$. These eigenvalues provide two distinct eigenvectors,
 120 forming a basis in which the full system (1) is uncoupled and, therefore, has a straight-forward
 121 solution. The eigensolutions T_{\pm} are the solutions associated with each eigenvalue. Afterwards,
 122 one can return to the original representation, finding that T_u and T_d are linear combinations of
 123 T_{\pm} . These linear combinations are the normal modes: the symmetric mode $T_s := T_+ + T_-$ and the
 124 antisymmetric mode $T_a := T_+ - T_-$. The main result of this process is that $T_u = T_s$ and $T_d = \alpha T_s + \beta T_a$,
 125 where α and β are scalars that depend on the coefficients of the system (1). The normal-mode
 126 representation again reveals the intricate coupling of the deep layer with the upper layer. Despite
 127 Geoffroy et al. (2013a); Rohrschneider et al. (2019) discuss the solutions extensively, they do not
 128 put them in terms of the normal modes. They did not overlooked this form of the solutions but
 129 was not necessary for their research questions. Nonetheless, for this work, the normal modes are
 130 fundamental.

131 3. Results

132 (i) *The explicit slope of the NT–diagram* From the solutions to system (1) written in terms of the
 133 normal modes, one can obtain an expression for the slope of the NT–diagram, \dot{N}/\dot{T}_u , of a system
 134 under constant forcing. In the appendix, I derive the following closed expression for the slope
 135 in terms of the derivatives of the normal modes and as a factor of the constant climate feedback
 136 parameter λ

$$137 \frac{\dot{N}}{\dot{T}_u} = \left\{ \frac{\varepsilon + 1}{2\varepsilon} + \frac{\varepsilon - 1}{2\varepsilon} \frac{C_u \kappa}{|\lambda|} \left[\left(\frac{\varepsilon}{C_u} + \frac{1}{C_d} \right) \frac{\gamma}{\kappa} - \frac{\dot{T}_a}{\dot{T}_s} \right] \right\} \lambda \quad (2)$$

138
 139 The main characteristic of equation (2) is the square-bracket term of its right-hand side. It contains
 140 two parts. The first one sets a basic enhanced slope and contains the sum of the inverse of the

141 thermal capacities as if we had an electrical circuit with capacitors in series. The second part
 142 provides the time evolution. It is a ratio of the changes in energy content. This ratio compares the
 143 change in energy content of the deep layer with that of the upper layer. To confirm the importance
 144 of the square-bracket term, one can take the limit as $\varepsilon \rightarrow 1$, where the pattern effect is cancelled in
 145 equation (2)

$$146 \quad \lim_{\varepsilon \rightarrow 1} \frac{\dot{N}}{\dot{T}_u} = \lambda$$

147
 148 The strong coupling between the upper and deep layers disappears. We end up with a constant
 149 slope. However, if $\varepsilon \neq 1$, the climate feedback parameter varies with the ratio of the changes in
 150 energy content from the deep to the upper layer around a basic value that depends on the thermal
 151 capacities of the system, the square bracket term in equation (2).

152 *(ii) Explicit expression for the ratio term* Using explicit expressions for T_s and T_a of an experiment
 153 with constant forcing, I write the ratio term in equation (2) as

$$154 \quad \frac{\dot{T}_a}{\dot{T}_s} = \tanh \left[\frac{\kappa}{2}(t - t_0) + \operatorname{arctanh} \left(\frac{\hat{\lambda} + 2\gamma'_d}{\kappa} \right) \right] \quad (3)$$

155
 156 The ratio (3) grows in a sigmoidal fashion from -1 to 1 . This hyperbolic tangent has a scaling
 157 factor $(\kappa/2)$ that sets the rate of change of the hyperbolic tangent between its extreme values. It also
 158 has a shift (the $\operatorname{arctanh}$ term) that determines when the hyperbolic tangent crosses zero, governing
 159 the contribution of the last term in equation (2). Both scaling and shift are in terms of the thermal
 160 capacities, the reference rate of deep-ocean enthalpy uptake γ and the reference climate feedback
 161 parameter λ .

162 The interpretation of equation (3) is that, after the initial forcing, the deep ocean warms up
 163 slower than the upper layer, steepening the slope of the NT -diagram. Once the ratio reaches
 164 the sign-reversal point, the last term's contribution in equation (2) only flattens the slope of the
 165 NT -diagram. The scaling factor and the shift of the ratio (3) set the timescale for the flattening.

166 Equation (3) expresses precisely the time evolution of the climate feedback parameter that others
 167 have only guessed through numerical experiments with the modified two-layer model (Geoffroy
 168 et al. 2013a; Rohrschneider et al. 2019). Additionally, it establishes a third timescale in the Earth
 169 system, related to the atmosphere-ocean coupling.

170 (iii) *Explicit expression of the climate feedback parameter* With the explicit expressions, I present
 171 you equation (2) for the climate feedback parameter

$$172 \quad \frac{\dot{N}}{\dot{T}_u} = \frac{\varepsilon + 1}{2\varepsilon} \left(1 + \frac{\varepsilon - 1}{\varepsilon + 1} \frac{C_u \kappa}{|\lambda|} \left[\left(\frac{\varepsilon}{C_u} + \frac{1}{C_d} \right) \frac{\gamma}{\kappa} - \tanh \left(\frac{\kappa}{2} (t - t_0) + \operatorname{arctanh} \left(\frac{\hat{\lambda} + 2\gamma'_d}{\kappa} \right) \right) \right] \right) \lambda \quad (4)$$

174 The factor of the constant λ is composed of terms that are positive except for the ratio term
 175 coming from equation (3). One can prove that at the start ($t = t_0$) the slope is

$$176 \quad \frac{\dot{N}}{\dot{T}_u}(t_0) = \left(1 + (\varepsilon - 1) \frac{\gamma}{|\lambda|} \right) \lambda$$

178 and from here up to the sign reversal of the ratio term, the slope flattens. The flattening is gentle
 179 at first, but towards the sign reversal it accelerates.

180 At the time of sign reversal we have

$$181 \quad \frac{\dot{N}}{\dot{T}_u}(t_{\text{rev}}) = \frac{\varepsilon + 1}{2\varepsilon} \left(1 + \frac{\varepsilon - 1}{\varepsilon + 1} \left(\frac{\varepsilon}{C_u} + \frac{1}{C_d} \right) \frac{C_u \gamma}{|\lambda|} \right) \lambda$$

183 and from here and on, the ratio term becomes positive, leading to an even flatter slope. The flattening
 184 decelerates and becomes gentle again. The asymptotic value of the slope of the NT -diagram is

$$185 \quad \lim_{t \rightarrow \infty} \frac{\dot{N}}{\dot{T}_u} = \frac{\varepsilon + 1}{2\varepsilon} \left(1 + \frac{\varepsilon - 1}{\varepsilon + 1} \frac{C_u \kappa}{|\lambda|} \left[\left(\frac{\varepsilon}{C_u} + \frac{1}{C_d} \right) \frac{\gamma}{\kappa} - 1 \right] \right) \lambda$$

187 (iv) *Numerical estimates of the atmosphere-ocean coupling* By substituting in expression (4)
 188 the parameter values found by Geoffroy et al. (2013a), I find the timescale for the sign reversal
 189 of the \dot{T}_a/\dot{T}_s ratio term. This timescale is important because it determines the middle of the
 190 transition between the initial and final values of the slope. I use the multimodel mean values

191 reported by Geoffroy et al. (2013a). For the multimodel average values ($C_u = 8.2 \text{ W yr m}^{-2} \text{ K}^{-1}$,
192 $C_d = 109 \text{ W yr m}^{-2} \text{ K}^{-1}$, $\gamma = 0.67 \text{ W m}^{-2} \text{ K}^{-1}$, $\lambda = -1.18 \text{ W m}^{-2} \text{ K}^{-1}$ and $\varepsilon = 1.28$) the sign reversal
193 of the ratio term takes place after 18.3 years. This timescale lies between the fast (4.2 years) and
194 slow (290 years) timescales established in terms of the thermal capacities alone (Geoffroy et al.
195 2013a).

196 I calculate the time for sign reversal using the rest of values in the tables of Geoffroy et al. (2013a)
197 and obtain that the multimodel average is 18.8 years. The minimum value is 8.8 years for GISS-
198 E2-R, whereas the maximum is 25.1 years for CNRM-CM5.1. If I compare with their estimates
199 of the fast and the slow timescales, even the extreme values fit well between both. Enlightening is
200 that the timescale of the sign reversal seems to fit with the de-facto 20-year standard to evaluate
201 the change in slope (e.g. Ceppi and Gregory 2017).

202 I also compare between the multimodel averages for all parameters and with the thermal ca-
203 pacities as calculated by Jiménez-de-la-Cuesta and Mauritsen (2019): $C_u = 7.2 \text{ W yr m}^{-2} \text{ K}^{-1}$,
204 $C_d = 367 \text{ W yr m}^{-2} \text{ K}^{-1}$. The calculated deep-layer thermal capacity is larger than the CMIP5
205 multi-model average, whereas the calculated value for the upper layer is smaller than the CMIP5
206 average. From these differences, we can note changes in the slope evolution (figure 2). Although
207 the difference in final slopes is small, the calculated thermal capacities strongly shift the sign-
208 reversal timescale: a deeper deep ocean lengthens the sign-reversal timescale, whereas a shallower
209 upper layer shortens it.

210 **4. Analysis and Discussion**

211 *(i) Consequences of an enthalpy-uptake interpretation* We have two terms in the factor of equation
212 (4): the identity term and the $(\varepsilon - 1)$ -term. The second term is only active if $\varepsilon \neq 1$, and has two
213 contributions. The first one is a constant contribution linked to the thermal capacities of the system.

214 The second contribution is time-varying and depends on the ratio \dot{T}_a/\dot{T}_s . This ratio measures the
215 proportion of energy that goes into the deep ocean compared to that stored in the upper layer.
216 Together, these terms provide a physical picture in which the slope's variation is determined by a
217 basic thermal capacity, which is expanded. The expansion stems from the enthalpy fluxes of the
218 upper and deep layers, which is better connected with the spatio-temporal warming pattern than
219 with the atmospheric feedbacks, given that the evolution and spatial distribution of the sea surface
220 temperature corresponds to changes in the enthalpy fluxes.

221 Precisely, I showed above that the thermal capacities have a strong effect on the timescale at
222 which the slope of the NT -diagram changes (figure 2). Thermal capacities in complex models
223 depend strongly on the depth of the ocean mixed-layer and, therefore, on the atmosphere-ocean
224 coupling, providing diverse behaviours (figure 3)

225 The consequences in the real Earth System of what I presented above are that the relative change
226 in the energy fluxes due to the atmosphere-ocean coupling compels the atmospheric feedbacks to
227 adjust. Thus, the magnitude of the changes in the atmospheric radiative response needs knowledge
228 of the physics of the atmosphere-ocean coupling. In summary, the prevailing interpretation of the
229 effect of the spatio-temporal warming pattern as additional fictitious "deep-ocean-driven" feedback
230 mechanisms depending on T_d is artificial. Then, uncertainties in our knowledge about the nature
231 of the atmosphere-ocean coupling can play a larger role than thought before (Kiehl 2007).

232 When comparing prescribed-sea-surface-temperature with fully-coupled numerical experiments
233 in complex climate models, there are striking differences in radiation and precipitation related to
234 differing sea surface temperature patterns between both settings. Therefore, in the light of the
235 results that I presented, the ocean circulation and the enthalpy transport representations in the
236 fully-coupled complex models could be key factors impacting the radiative response.

237 (ii) *State and forcing dependence* In this article, I ignored the dependence on the strength of
 238 forcing (Senior and Mitchell 2000; Meraner et al. 2013; Rohrschneider et al. 2019). However, such
 239 dependence should come from the reference values ε , λ and γ that are particular to a given forcing.
 240 Values of λ and γ are first-order derivatives in the neighbourhood of the starting states. The same
 241 goes for ε . Therefore, we need to connect ε to the physics of the real atmospheric-oceanic coupling,
 242 possibly circulation, to understand its effect in the variation of the slope of the NT -diagrams under
 243 different forcings. We need to answer how the forcing impacts the atmosphere-ocean coupling
 244 resulting in another spatio-temporal warming pattern.

245 There are versions of linearised energy balance models in which a simple non-linear term is
 246 introduced (Rohrschneider et al. 2019). Although higher-order terms in the Taylor expansion of
 247 either the radiative response R or the enthalpy uptake H can provide additional information on state
 248 dependence, the temporal dependencies arising from the atmosphere-ocean coupling, as shown in
 249 this article, are far more important in light of the results presented above. These results shift the
 250 limelight to the physics of the atmosphere-ocean coupling.

251 (iii) *Non-linear planetary energy balance* Above I presented evidence favouring the ocean's
 252 enthalpy uptake central role in determining the spatio-temporal warming pattern and its effects on
 253 the atmospheric feedback mechanisms. I test this idea in a more general theoretical framework by
 254 writing the planetary energy budget in another widely-known incarnation

$$255 \quad N = (1 - \alpha)S + G - \epsilon\sigma(fT_u)^4 \quad (5)$$

257 where $S := S(t)$ in W m^{-2} is the incoming solar radiative flux at the TOA, α is the planetary albedo,
 258 $G := G(t)$ in W m^{-2} represents the remaining inputs (natural and anthropogenic), and the last term
 259 is the usual planetary longwave emission, in W m^{-2} , as a grey-body of emissivity ϵ and surface
 260 temperature T_u with f the lapse-rate scaling factor for the emission temperature. At first inspection,

261 we have the origin of the feedback mechanisms: the planetary albedo α , the emissivity ϵ and the
 262 scaling factor f . On the one hand, we have the shortwave strand, the albedo $\alpha := \alpha(T_u, q_{cl,d,w}, \dots)$
 263 that is a function of, e.g., the surface temperature and the amount of liquid water in the atmosphere
 264 forming clouds. On the other hand, we have the longwave thread, the emissivity and the lapse-
 265 rate scaling factor $\epsilon, f := f(T_u, q_v, q_{cl,d,w}, \dots)$, depending on, e.g. the surface temperature, and the
 266 amount of water vapour and cloud liquid water in the atmosphere.

267 The atmospheric feedback mechanisms cannot rely on any temperature we define inside the
 268 ocean. The ocean affects α, ϵ and f only through changing T_u . In equation (5), we cannot see such
 269 dependence. Therefore, here we would be tempted to artificially introduce it by saying that α, ϵ
 270 and f depend on another temperature in the ocean, as others have interpreted from the modified
 271 two-layer model. In this work, I have shown that there is another more natural place where the
 272 ocean enters into play: the energy imbalance at the TOA, N . Some would naively say that $N = C\dot{T}_u$
 273 only, with C the planetary thermal capacity per unit area. My results suggest a more precise
 274 incarnation of this term: $N = (d/dt)(CT_u)$, because we do not know if C varies with time. We
 275 have no *a priori* basis to say that it is constant. It depends on, e.g., the thickness of the ocean's
 276 mixed-layer, the depth of the thermally-active deep-ocean or the melted volume of the ice sheet.
 277 The spatio-temporal warming pattern may also depend on these variables. Thus, how does the
 278 term N look like? $N = C\dot{T}_u + \dot{C}T_u$. If we rewrite the equation (5) with this new information

$$279 \quad C\dot{T}_u = (1 - \alpha)S + G - \epsilon\sigma(fT_u)^4 - \dot{C}T_u \quad (6)$$

281 where the term $C\dot{T}_u$ is an effective N . The last term of equation (6) is the representation of the
 282 effect of the spatio-temporal warming pattern. The factor \dot{C} needs a new differential equation
 283 that describes the temporal variations of the enthalpy uptake due to the ocean and the melting
 284 ice sheets. When linearising, this term will be transformed in the $(1 - \epsilon)H$ term of the planetary

285 energy imbalance of system (1). In other words, the $\dot{C}T_u$ term embodies the radiative effect of the
286 atmosphere-ocean coupling.

287 5. Conclusions

288 I presented for the first time an explicit mathematical expression for the slope of the NT -diagrams
289 using the linearised framework of the modified two-layer energy balance model. In particular, I
290 presented an expression applicable to the case of experiments in which we increment the atmo-
291 spheric carbon dioxide concentration up to n times the pre-industrial levels. From the analysis of
292 the solutions of the modified two-layer energy balance model and the mathematical expression for
293 the slope, I concluded that the evolution of the climate feedback parameter comes from a ratio
294 that compares the changes in the energy content of the deep ocean in relation to those of the
295 upper layer. This ratio modulates the slope change around a basic state. The thermal capacities
296 and the efficacy parameter determine this basic state, shifting away from the usual focus on the
297 atmospheric feedback mechanisms and their dependence on another temperature in the ocean (T_d).
298 Thus, in the context of complex climate models and observations, I show that the variation of the
299 climate feedback parameter is a direct consequence of the atmosphere-ocean coupling that gives
300 rise to the spatio-temporal warming pattern. The spatio-temporal warming pattern shows how the
301 enthalpy is exchanged between the atmosphere and the ocean. The atmosphere-ocean coupling
302 modifies the surface temperature, and the feedback mechanisms adjust to this external change.
303 Therefore, the variation of the feedback mechanisms provides partial and indirect information on
304 the spatio-temporal warming pattern. To fill the gap, we need information on the physics of the
305 atmosphere-ocean coupling: its relation to circulation and the generation of the spatio-temporal
306 warming pattern.

307 *Acknowledgments.* I thank Hauke Schmidt, Jiawei Bao and Moritz Gunther for reading and
308 correcting the manuscript and for the lively discussions on how to present this highly theoretical
309 ideas.

310 *Data availability statement.* All the data used by this study is described fully in the main text.
311 The numbers for reproducing the figure 2 and 3 are contained in the articles by Geoffroy et al.
312 (2013a) and Jiménez-de-la-Cuesta and Mauritsen (2019). The theoretical considerations are fully
313 described in the appendix to this article. Therefore, this article fully reproducible and almost self
314 contained.

315 APPENDIX

316 In Classical Mechanics, a very coarse thinking would be reducing the field to the task of solving
317 the equation $\dot{\mathbf{p}} = \mathbf{F}$ for any force term, either analytically or numerically. Going further leads to
318 conservation principles and formulations of Classical Mechanics that provide more information
319 without actually obtaining solutions, if that is possible at all. In this appendix, reduced to the scale
320 of a simplified framework, I show that by delving deep into the mathematics of a system of linear
321 ordinary differential equations, the structure of the solutions and the its physical interpretation, one
322 can obtain a new view on an old problem.

323 The appendix is written in an exhaustive way and I leave few things without development. The
324 cases in which I do not show some algebraic step is because the necessary step has been already
325 done or is very simple.

326 Matrix form of the equations

327 The equations of two-layer model Geoffroy et al. (2013a) are

$$\begin{aligned}
 328 \quad N_u &= C_u \dot{T}_u = F + \lambda T_u - \varepsilon \gamma (T_u - T_d) \\
 329 \quad N_d &= C_d \dot{T}_d = \gamma (T_u - T_d)
 \end{aligned} \tag{A1}$$

330 and the planetary imbalance is $N = N_u + N_d$. I present another form of the equations, where I divide
 331 by the thermal capacities.

$$\begin{aligned}
 332 \quad \dot{T}_u &= \frac{F}{C_u} + \frac{\lambda}{C_u} T_u - \varepsilon \frac{\gamma}{C_u} (T_u - T_d) \\
 333 \quad \dot{T}_d &= \frac{\gamma}{C_d} (T_u - T_d)
 \end{aligned}$$

334 If I define $F' := F/C_u$, $\lambda' := \lambda/C_u$, $\gamma' := \gamma/C_u$, $\gamma'_d := \gamma/C_d$, one can write the equations in a lean
 335 way

$$\begin{aligned}
 336 \quad \dot{T}_u &= F' + \lambda' T_u - \varepsilon \gamma' (T_u - T_d) \\
 337 \quad \dot{T}_d &= \gamma'_d (T_u - T_d)
 \end{aligned} \tag{A2}$$

338 I will put the system in matrix form. I define $\mathbf{T} := (T_u, T_d)$, $\mathbf{F}' := (F', 0)$ and

$$339 \quad \mathbf{A} := \begin{pmatrix} \lambda' - \varepsilon \gamma' & \gamma'_d \\ \varepsilon \gamma' & -\gamma'_d \end{pmatrix} \tag{A3}$$

340 and the system can be written

$$342 \quad \dot{\mathbf{T}} = \mathbf{F}' + \mathbf{T}\mathbf{A} \tag{A4}$$

343 which is the representation of the system in the temperature basis.

345 Eigenvalues and eigenvectors

346 I want to analyse the normal modes of the system. For that end, I need the eigenvalues of the
 347 homogeneous system obtained as the solutions of the characteristic equation

$$348 \quad (\lambda' - \varepsilon \gamma' - \mu)(-\gamma'_d - \mu) - \varepsilon \gamma' \gamma'_d = 0 \tag{A5}$$

349

$$-\lambda' \gamma'_d + \varepsilon \gamma' \gamma'_d + \mu \gamma'_d - \lambda' \mu + \varepsilon \gamma' \mu + \mu^2 - \varepsilon \gamma' \gamma'_d = 0$$

$$-\lambda' \gamma'_d + \mu \gamma'_d - \lambda' \mu + \varepsilon \gamma' \mu + \mu^2 = 0$$

$$-\lambda' \gamma'_d - (\lambda' - \varepsilon \gamma' - \gamma'_d) \mu + \mu^2 = 0$$

The solutions of equation (A5) are

$$\mu = \frac{(\lambda' - \varepsilon \gamma' - \gamma'_d) \pm [(\lambda' - \varepsilon \gamma' - \gamma'_d)^2 + 4\lambda' \gamma'_d]^{1/2}}{2} \quad (\text{A6})$$

and, given that in the Earth $C_u < C_d$, one can prove that there are two real and different eigenvalues. One needs to check that the square root term is not complex or zero. This only happens if the sum within the square root is negative or zero

$$(\lambda' - \varepsilon \gamma' - \gamma'_d)^2 + 4\lambda' \gamma'_d \leq 0$$

$$(\lambda' - \varepsilon \gamma')^2 - 2(\lambda' - \varepsilon \gamma') \gamma'_d + \gamma'_d{}^2 + 4\lambda' \gamma'_d \leq 0$$

$$\lambda'^2 - 2\lambda' \varepsilon \gamma' + (\varepsilon \gamma')^2 - 2(\lambda' - \varepsilon \gamma') \gamma'_d + \gamma'_d{}^2 + 4\lambda' \gamma'_d \leq 0$$

$$\lambda'^2 - 2\lambda' \varepsilon \gamma' + (\varepsilon \gamma')^2 - 2\lambda' \gamma'_d + 2\varepsilon \gamma' \gamma'_d + \gamma'_d{}^2 + 4\lambda' \gamma'_d \leq 0$$

$$(\lambda' / \gamma'_d)^2 - 2(\lambda' / \gamma'_d) \varepsilon (\gamma' / \gamma'_d) + (\varepsilon (\gamma' / \gamma'_d))^2 + 2\varepsilon (\gamma' / \gamma'_d) + 1 + 2(\lambda' / \gamma'_d) \leq 0$$

$$(\lambda' / \gamma'_d)^2 - 2(\lambda' / \gamma'_d) [\varepsilon (\gamma' / \gamma'_d) - 1] + (\varepsilon (\gamma' / \gamma'_d))^2 + 2\varepsilon (\gamma' / \gamma'_d) + 1 \leq 0$$

$$(\lambda' / \gamma'_d)^2 - 2(\lambda' / \gamma'_d) [\varepsilon (\gamma' / \gamma'_d) - 1] + (\varepsilon (\gamma' / \gamma'_d) + 1)^2 \leq 0$$

$$(\lambda' / \gamma'_d)^2 + (\varepsilon (C_d / C_u) + 1)^2 \leq 2(\lambda' / \gamma'_d) [\varepsilon (C_d / C_u) - 1]$$

In the last inequality, the left-hand side is always positive. The right-hand side depends on the sign of the factors. The middle factor is negative since λ' is negative and γ'_d is positive. The third factor is positive provided that $\varepsilon > C_u / C_d$. Given that $\varepsilon \geq 1$ and $C_u < C_d$, then the third factor is positive in our case. Then the right-hand side is negative. Thus, we obtained a contradiction by

374 supposing that the square root term was negative or zero. Therefore, the conclusion is that the
 375 eigenvalues are two real and distinct numbers.

376 I call the solutions μ_+ and μ_- , depending on the sign of the square root term. Let us rewrite their
 377 expression in more lean fashion. I define $\hat{\lambda} := \lambda' - \varepsilon\gamma' - \gamma'_d$ and we call κ the square root term.
 378 Then, I rewrite the solutions (A6) as

$$379 \mu_{\pm} = \frac{\hat{\lambda} \pm \kappa}{2} \quad (A7)$$

381 Now that I know the eigenvalues, one should get the eigenvectors of the system and solve it
 382 easily. The eigenvectors are the generators of the kernel of the operators $\mathbf{A} - \mu_{\pm} \text{id}$. Let us write
 383 the diagonal of the matrix \mathbf{A} with the definition of $\hat{\lambda}$

$$384 \mathbf{A} = \begin{pmatrix} \hat{\lambda} + \gamma'_d & \gamma'_d \\ \varepsilon\gamma' & \hat{\lambda} - (\lambda' - \varepsilon\gamma') \end{pmatrix}$$

386 and then the matrices for each eigenvalue have the form

$$387 \mathbf{A} - \mu_{\pm} \text{id} = \begin{pmatrix} \hat{\lambda} + \gamma'_d - \mu_{\pm} & \gamma'_d \\ \varepsilon\gamma' & \hat{\lambda} - (\lambda' - \varepsilon\gamma') - \mu_{\pm} \end{pmatrix}$$

$$388 = \begin{pmatrix} \mu_{\mp} + \gamma'_d & \gamma'_d \\ \varepsilon\gamma' & \mu_{\mp} - (\lambda' - \varepsilon\gamma') \end{pmatrix}$$

390 Since eigenvalues are real and distinct, there should be two linearly-independent eigenvectors,
 391 one for each eigenvalue. These vectors should fulfill that $\mathbf{e}_{\pm}(\mathbf{A} - \mu_{\pm} \text{id}) = 0$. Solving that linear
 392 system, I find the eigenvectors in temperature representation

$$393 \mathbf{e}_{\pm} = \mathbf{e}_u - \frac{\mu_{\mp} + \gamma'_d}{\varepsilon\gamma'} \mathbf{e}_d \quad (A8)$$

395 The procedure to get the result is to solve the system of homogeneous linear equations $\mathbf{e}_{\pm}(\mathbf{A} -$
 396 $\mu_{\pm} \text{id}) = 0$

$$397 \quad \begin{cases} (\mu_{\mp} + \gamma'_d)e_{\pm,u} & + \varepsilon\gamma'e_{\pm,d} = 0 \\ \gamma'_de_{\pm,u} + [\mu_{\mp} - (\lambda' - \varepsilon\gamma')]e_{\pm,d} = 0 \end{cases}$$

399 I solve the first equation for the component $e_{\pm,d}$, and substitute this result on the second equation

$$400 \quad e_{\pm,d} = -\frac{\mu_{\mp} + \gamma'_d}{\varepsilon\gamma'}e_{\pm,u} \longrightarrow$$

$$401 \quad \left(\gamma'_d - \frac{[\mu_{\mp} - (\lambda' - \varepsilon\gamma')](\mu_{\mp} + \gamma'_d)}{\varepsilon\gamma'} \right) e_{\pm,u} = 0$$

$$402 \quad \frac{\varepsilon\gamma'\gamma'_d - [\mu_{\mp} - (\lambda' - \varepsilon\gamma')](\mu_{\mp} + \gamma'_d)}{\varepsilon\gamma'} e_{\pm,u} = 0, (\varepsilon, \gamma' \neq 0) \therefore$$

$$405 \quad \{ \varepsilon\gamma'\gamma'_d - [\mu_{\mp} - (\lambda' - \varepsilon\gamma')](\mu_{\mp} + \gamma'_d) \} e_{\pm,u} = 0$$

$$406 \quad \{ \varepsilon\gamma'\gamma'_d + [(\lambda' - \varepsilon\gamma') - \mu_{\mp}](\gamma'_d + \mu_{\mp}) \} e_{\pm,u} = 0$$

$$407 \quad - \{ -\varepsilon\gamma'\gamma'_d + [(\lambda' - \varepsilon\gamma') - \mu_{\mp}](-\gamma'_d - \mu_{\mp}) \} e_{\pm,u} = 0$$

409 and in the last expression we have two options: either $e_{\pm,u}$ is zero or the term within curly braces is
 410 zero. However, the expression in curly braces is the characteristic equation (A5) and then always
 411 vanishes identically. This means that $e_{\pm,u} = \alpha \in \mathbb{R}$ can be chosen arbitrarily. I plug in this result in
 412 the expression for $e_{\pm,d}$ and get that

$$413 \quad e_{\pm,u} = \alpha$$

$$414 \quad e_{\pm,d} = -\frac{\mu_{\mp} + \gamma'_d}{\varepsilon\gamma'}\alpha$$

416 or as a vector in the temperature basis

$$417 \quad \mathbf{e}_{\pm} = e_{\pm,u}\mathbf{e}_u + e_{\pm,d}\mathbf{e}_d$$

$$418 \quad \mathbf{e}_{\pm} = \alpha\mathbf{e}_u - \frac{\mu_{\mp} + \gamma'_d}{\varepsilon\gamma'}\alpha\mathbf{e}_d$$

420 and since α is arbitrary this means we are in front of a subspace of vectors. I choose a basis by
 421 selecting $\alpha = 1$.

$$422 \quad \mathbf{e}_{\pm} = \mathbf{e}_u - \frac{\mu_{\mp} + \gamma'_d}{\varepsilon\gamma'} \mathbf{e}_d$$

424 which is the same as the equation (A8).

425 Now, I can derive the expressions of the temperature basis vectors in terms of the two eigenvectors.

426 If one solves for e_u in equation (A8)

$$427 \quad \mathbf{e}_{\pm} + \frac{\mu_{\mp} + \gamma'_d}{\varepsilon\gamma'} \mathbf{e}_d = \mathbf{e}_u$$

429 but we have here two expressions in a condensed way. Therefore,

$$430 \quad \mathbf{e}_- + \frac{\mu_+ + \gamma'_d}{\varepsilon\gamma'} \mathbf{e}_d = \mathbf{e}_+ + \frac{\mu_- + \gamma'_d}{\varepsilon\gamma'} \mathbf{e}_d$$

$$431 \quad \left(\frac{\mu_+ + \gamma'_d}{\varepsilon\gamma'} - \frac{\mu_- + \gamma'_d}{\varepsilon\gamma'} \right) \mathbf{e}_d = \mathbf{e}_+ - \mathbf{e}_-$$

$$432 \quad \frac{(\mu_+ + \gamma'_d) - (\mu_- + \gamma'_d)}{\varepsilon\gamma'} \mathbf{e}_d = \mathbf{e}_+ - \mathbf{e}_-$$

$$433 \quad \frac{\mu_+ - \mu_-}{\varepsilon\gamma'} \mathbf{e}_d = \mathbf{e}_+ - \mathbf{e}_-$$

$$434 \quad \mathbf{e}_d = \frac{\varepsilon\gamma'}{\mu_+ - \mu_-} (\mathbf{e}_+ - \mathbf{e}_-)$$

436 Thus, I have expressed \mathbf{e}_d in terms of the eigenvectors.

437 Now, I substitute the last result on one of the expressions for \mathbf{e}_u .

$$438 \quad \mathbf{e}_+ + \frac{\mu_- + \gamma'_d}{\varepsilon\gamma'} \mathbf{e}_d = \mathbf{e}_u$$

$$439 \quad \mathbf{e}_+ + \frac{\mu_- + \gamma'_d}{\varepsilon\gamma'} \frac{\varepsilon\gamma'}{\mu_+ - \mu_-} (\mathbf{e}_+ - \mathbf{e}_-) = \mathbf{e}_u$$

$$440 \quad \mathbf{e}_+ + \frac{\mu_- + \gamma'_d}{\mu_+ - \mu_-} (\mathbf{e}_+ - \mathbf{e}_-) = \mathbf{e}_u$$

$$441 \quad \left(1 + \frac{\mu_- + \gamma'_d}{\mu_+ - \mu_-}\right) \mathbf{e}_+ - \frac{\mu_- + \gamma'_d}{\mu_+ - \mu_-} \mathbf{e}_- = \mathbf{e}_u$$

$$442 \quad \frac{\mu_+ - \mu_- + \mu_- + \gamma'_d}{\mu_+ - \mu_-} \mathbf{e}_+ - \frac{\mu_- + \gamma'_d}{\mu_+ - \mu_-} \mathbf{e}_- = \mathbf{e}_u$$

$$443 \quad \frac{\mu_+ + \gamma'_d}{\mu_+ - \mu_-} \mathbf{e}_+ - \frac{\mu_- + \gamma'_d}{\mu_+ - \mu_-} \mathbf{e}_- = \mathbf{e}_u$$

444

445 and the temperature basis vectors in the eigenvector representation are

$$446 \quad \mathbf{e}_u = \frac{\mu_+ + \gamma'_d}{\mu_+ - \mu_-} \mathbf{e}_+ - \frac{\mu_- + \gamma'_d}{\mu_+ - \mu_-} \mathbf{e}_- \tag{A9}$$

$$447 \quad \mathbf{e}_d = \frac{\varepsilon\gamma'}{\mu_+ - \mu_-} (\mathbf{e}_+ - \mathbf{e}_-)$$

448

448 **Matrix in the eigenvector representation. Solutions**

449 With these results, I can write the matrix \mathbf{A} (A3) in the eigenvector basis and it should be the
450 following diagonal matrix

$$451 \quad \mathbf{B} = \begin{pmatrix} \mu_+ & 0 \\ 0 & \mu_- \end{pmatrix} \tag{A10}$$

452

453 I show how to get to this result. Let subscripts represent rows and superscripts represent columns.

454 I define that latin indices (i, j, k, \dots) have the possible values u, d ; and greek indices $(\alpha, \beta, \zeta, \dots)$

455 have possible values $+, -$. Also, repeated indices in expressions mean summation over the set of

456 possible values. With these considerations, equation (A9) is

$$457 \quad \mathbf{e}_i = \Lambda_i^\alpha \mathbf{e}_\alpha$$

458

459 where the rows of matrix Λ contain the coordinates of each of the vectors of the temperature basis
 460 in the eigenvector representation. Analogously, equation (A8) is

$$461 \quad \mathbf{e}_\alpha = \Theta_\alpha^i \mathbf{e}_i$$

463 where matrix Θ has in its rows the coordinates the eigenvector basis in the temperature represen-
 464 tation. This means that

$$465 \quad \mathbf{e}_\alpha = \Theta_\alpha^i \mathbf{e}_i = \Theta_\alpha^i \Lambda_i^\beta \mathbf{e}_\beta$$

467 which is only possible if the matrices Λ and Θ are inverse of each other

$$468 \quad \mathbf{e}_\alpha = \delta_\alpha^\beta \mathbf{e}_\beta = \mathbf{e}_\alpha$$

470 Thus, we write $\Theta = \Lambda^{-1}$.

471 Now, matrix \mathbf{A} is a representation of a linear operator f in the temperature representation. If
 472 $\mathbf{v} = v^j \mathbf{e}_j$ is a vector in the temperature representation, then the action of the linear operator f should
 473 be $f(\mathbf{v}) = f(v^j \mathbf{e}_j) = v^j f(\mathbf{e}_j)$. Then the action of f on a vector expressed in a given basis depends
 474 only on the action of the operator on the basis. Thus, $f(\mathbf{v}) = f(v^j \mathbf{e}_j) = v^j f(\mathbf{e}_j) = v^j \mathbf{A}_j^k \mathbf{e}_k$. Thus
 475 the matrix \mathbf{A} has in its rows the coordinates in the temperature representation of the action of f
 476 over each basis vector. Once one understands what is happening under the hood, what we want
 477 is the matrix \mathbf{B} , which is the representation of f in the eigenvector basis. Therefore, I begin with
 478 the basic relationship in the temperature representation and introduce the change of representation

479 using the alternative representation of equations (A8) and (A9)

$$480 \quad f(\mathbf{e}_i) = \mathbf{A}_i^j \Lambda_j^\zeta \mathbf{e}_\zeta$$

$$481 \quad f(\Lambda_i^\alpha \mathbf{e}_\alpha) = \mathbf{A}_i^j \Lambda_j^\zeta \mathbf{e}_\zeta$$

$$482 \quad \Lambda_i^\alpha f(\mathbf{e}_\alpha) = \mathbf{A}_i^j \Lambda_j^\zeta \mathbf{e}_\zeta$$

$$483 \quad (\Lambda^{-1})_\beta^i \Lambda_i^\alpha f(\mathbf{e}_\alpha) = (\Lambda^{-1})_\beta^i \mathbf{A}_i^j \Lambda_j^\zeta \mathbf{e}_\zeta$$

$$484 \quad f(\mathbf{e}_\beta) = (\Lambda^{-1})_\beta^i \mathbf{A}_i^j \Lambda_j^\zeta \mathbf{e}_\zeta, f(\mathbf{e}_\beta) := \mathbf{B}_\beta^\zeta \mathbf{e}_\zeta$$

$$485 \quad \mathbf{B}_\beta^\zeta = (\Lambda^{-1})_\beta^i \mathbf{A}_i^j \Lambda_j^\zeta$$

487 or in matrix notation $\mathbf{B} = \Lambda^{-1} \mathbf{A} \Lambda$. Then, I multiply the matrices

$$488 \quad \Lambda^{-1} = \begin{pmatrix} 1 & -\frac{\mu_- + \gamma'_d}{\varepsilon \gamma'} \\ 1 & -\frac{\mu_+ + \gamma'_d}{\varepsilon \gamma'} \end{pmatrix}, \mathbf{A} = \begin{pmatrix} \hat{\lambda} + \gamma'_d & \gamma'_d \\ \varepsilon \gamma' & -\gamma'_d \end{pmatrix}, \Lambda = \begin{pmatrix} \frac{\mu_+ + \gamma'_d}{\mu_+ - \mu_-} & -\frac{\mu_- + \gamma'_d}{\mu_+ - \mu_-} \\ \frac{\varepsilon \gamma'}{\mu_+ - \mu_-} & -\frac{\varepsilon \gamma'}{\mu_+ - \mu_-} \end{pmatrix}$$

490 First, note that $\mu_+ - \mu_- = \kappa$. One also looks at the following quantities that will help in the
 491 process: $\mu_+ + \mu_- = \hat{\lambda}$ and $\mu_+ \mu_- = \frac{1}{4}(\hat{\lambda}^2 - \kappa^2) = \frac{1}{4}(\hat{\lambda}^2 - \hat{\lambda}^2 - 4\lambda' \gamma'_d) = -\lambda' \gamma'_d$. I proceed with the first
 492 product, $\Lambda^{-1} \mathbf{A}$.

$$493 \quad \Lambda^{-1} \mathbf{A} = \begin{pmatrix} 1 & -\frac{\mu_- + \gamma'_d}{\varepsilon \gamma'} \\ 1 & -\frac{\mu_+ + \gamma'_d}{\varepsilon \gamma'} \end{pmatrix} \begin{pmatrix} \hat{\lambda} + \gamma'_d & \gamma'_d \\ \varepsilon \gamma' & -\gamma'_d \end{pmatrix}$$

$$494 \quad = \begin{pmatrix} \hat{\lambda} + \gamma'_d - \mu_- - \gamma'_d & \left(1 + \frac{\mu_- + \gamma'_d}{\varepsilon \gamma'}\right) \gamma'_d \\ \hat{\lambda} + \gamma'_d - \mu_+ - \gamma'_d & \left(1 + \frac{\mu_+ + \gamma'_d}{\varepsilon \gamma'}\right) \gamma'_d \end{pmatrix}$$

$$495 \quad = \begin{pmatrix} \hat{\lambda} - \mu_- & \frac{\varepsilon \gamma' + \mu_- + \gamma'_d}{\varepsilon \gamma'} \gamma'_d \\ \hat{\lambda} - \mu_+ & \frac{\varepsilon \gamma' + \mu_+ + \gamma'_d}{\varepsilon \gamma'} \gamma'_d \end{pmatrix}$$

$$496 \quad = \begin{pmatrix} \mu_+ & \frac{\varepsilon \gamma' + \mu_- + \gamma'_d}{\varepsilon \gamma'} \gamma'_d \\ \mu_- & \frac{\varepsilon \gamma' + \mu_+ + \gamma'_d}{\varepsilon \gamma'} \gamma'_d \end{pmatrix}$$

498 and multiply the result by Λ

$$\begin{aligned}
499 \quad \Lambda^{-1} \mathbf{A} \Lambda &= \begin{pmatrix} \mu_+ & \frac{\varepsilon \gamma' + \mu_- + \gamma'_d}{\varepsilon \gamma'} \gamma'_d \\ \mu_- & \frac{\varepsilon \gamma' + \mu_+ + \gamma'_d}{\varepsilon \gamma'} \gamma'_d \end{pmatrix} \begin{pmatrix} \frac{\mu_+ + \gamma'_d}{\mu_+ - \mu_-} & -\frac{\mu_- + \gamma'_d}{\mu_+ - \mu_-} \\ \frac{\varepsilon \gamma'}{\mu_+ - \mu_-} & -\frac{\varepsilon \gamma'}{\mu_+ - \mu_-} \end{pmatrix} \\
500 &= \frac{1}{\kappa} \begin{pmatrix} \mu_+^2 + \mu_+ \gamma'_d + \varepsilon \gamma' \gamma'_d + \mu_- \gamma'_d + \gamma_d'^2 & -\mu_+ \mu_- - \mu_+ \gamma'_d - \varepsilon \gamma' \gamma'_d - \mu_- \gamma'_d - \gamma_d'^2 \\ \mu_- \mu_+ + \mu_- \gamma'_d + \varepsilon \gamma' \gamma'_d + \mu_+ \gamma'_d + \gamma_d'^2 & -\mu_-^2 - \mu_- \gamma'_d - \varepsilon \gamma' \gamma'_d - \mu_+ \gamma'_d - \gamma_d'^2 \end{pmatrix} \\
501 &= \frac{1}{\kappa} \begin{pmatrix} \mu_+^2 + (\hat{\lambda} + \varepsilon \gamma' + \gamma'_d) \gamma'_d & -\mu_+ \mu_- - (\hat{\lambda} + \varepsilon \gamma' + \gamma'_d) \gamma'_d \\ \mu_- \mu_+ + (\hat{\lambda} + \varepsilon \gamma' + \gamma'_d) \gamma'_d & -\mu_-^2 - (\hat{\lambda} + \varepsilon \gamma' + \gamma'_d) \gamma'_d \end{pmatrix} \\
502 &= \frac{1}{\kappa} \begin{pmatrix} \mu_+^2 - \mu_+ \mu_- & \lambda' \gamma'_d - \lambda \gamma'_d \\ -\lambda' \gamma'_d + \lambda \gamma'_d & -\mu_-^2 + \mu_+ \mu_- \end{pmatrix} = \frac{1}{\kappa} \begin{pmatrix} \mu_+ \kappa & 0 \\ 0 & \mu_- \kappa \end{pmatrix} = \begin{pmatrix} \mu_+ & 0 \\ 0 & \mu_- \end{pmatrix} \\
503 & \\
504 &
\end{aligned}$$

504 the last line is the result that we wanted to check.

505 In the eigenvector representation the system (A4) has the following form

$$506 \quad \dot{\mathbf{T}} = \mathbf{F}' + \mathbf{T} \mathbf{B} \quad (A11)$$

508 and, therefore, is decoupled. Therefore, I can solve each equation separately. I need only to
509 transform the forcing vector to the eigenvector representation.

510 The equations are

$$511 \quad \dot{T}_{\pm} = F'_{\pm} + \mu_{\pm} T_{\pm}$$

513 and the solutions of a generic initial value problem are

$$514 \quad T_{\pm} = \left(T_{\pm,0} + \int_{t_0}^t F'_{\pm} e^{-\mu_{\pm}(\tau-t_0)} d\tau \right) e^{\mu_{\pm}(t-t_0)} \quad (A12)$$

516 where the initial values in the eigenvector representation in terms of the initial values in the
517 temperature representation are

$$518 \quad T_{\pm,0} = \pm \frac{1}{\mu_+ - \mu_-} [(\mu_{\pm} + \gamma'_d) T_{u,0} + \varepsilon \gamma' T_{d,0}]$$

519

520 the forcing components are

$$521 \quad F'_\pm = \pm \frac{\mu_\pm + \gamma'_d}{\mu_+ - \mu_-} F'$$

523 and the solutions in the temperature representation are

$$524 \quad T_u = T_+ + T_-$$

$$525 \quad T_d = -\frac{\mu_- + \gamma'_d}{\varepsilon\gamma'} T_+ - \frac{\mu_+ + \gamma'_d}{\varepsilon\gamma'} T_-$$

526 If I further expand the T_d solution, the form of the solutions is more elegant

$$527 \quad T_u = T_+ + T_- \tag{A13}$$

$$528 \quad T_d = -\frac{\hat{\lambda} + 2\gamma'_d}{2\varepsilon\gamma'} (T_+ + T_-) + \frac{\kappa}{2\varepsilon\gamma'} (T_+ - T_-)$$

529 since it shows that the solutions in the temperature space are in a sort of symmetric and antisymmet-
530 ric combinations of the solutions in the eigenvector representation. These are the normal modes.

531 One thing to note is that the upper temperature is the symmetric mode and the deep temperature is
532 a mixture of symmetric and antisymmetric modes.

533 I show how I got the solutions (A13). Just expand the T_d equation.

$$534 \quad T_d = -\frac{\mu_- + \gamma'_d}{\varepsilon\gamma'} T_+ - \frac{\mu_+ + \gamma'_d}{\varepsilon\gamma'} T_-$$

$$535 \quad = -\frac{1}{\varepsilon\gamma'} \left[\left(\frac{\hat{\lambda} - \kappa}{2} + \gamma'_d \right) T_+ + \left(\frac{\hat{\lambda} + \kappa}{2} + \gamma'_d \right) T_- \right]$$

$$536 \quad = -\frac{1}{\varepsilon\gamma'} \left[\left(\frac{\hat{\lambda} + 2\gamma'_d}{2} - \frac{\kappa}{2} \right) T_+ + \left(\frac{\hat{\lambda} + 2\gamma'_d}{2} + \frac{\kappa}{2} \right) T_- \right]$$

$$537 \quad = -\frac{1}{2\varepsilon\gamma'} [(\hat{\lambda} + 2\gamma'_d)(T_+ + T_-) - \kappa(T_+ - T_-)]$$

539 From now on, I write $T_s := T_+ + T_-$ and $T_a := T_+ - T_-$.

540 **Planetary imbalance**

541 Now, I will find an expression for the planetary imbalance in terms of the equations (A13). The

542 mathematical expression that I should expand is $N = N_u + N_d = C_u \dot{T}_u + C_d \dot{T}_d$

543
$$C_u \dot{T}_u = C_u \dot{T}_s$$

544
$$C_d \dot{T}_d = -C_d \frac{\hat{\lambda} + 2\gamma'_d}{2\varepsilon\gamma'} \dot{T}_s + C_d \frac{\kappa}{2\varepsilon\gamma'} \dot{T}_a \therefore$$

545
$$N = C_u \dot{T}_s - C_d \frac{\hat{\lambda} + 2\gamma'_d}{2\varepsilon\gamma'} \dot{T}_s + C_d \frac{\kappa}{2\varepsilon\gamma'} \dot{T}_a$$

546
$$= \left(C_u - C_d \frac{\hat{\lambda} + 2\gamma'_d}{2\varepsilon\gamma'} \right) \dot{T}_s + C_d \frac{\kappa}{2\varepsilon\gamma'} \dot{T}_a$$

547
$$= C_s \dot{T}_s + C_a \dot{T}_a$$

548

549 Now, $\dot{T}_\pm = F'_\pm + \mu_\pm T_\pm$, then

550
$$\dot{T}_s = \mu_+ T_+ + \mu_- T_- + (F'_+ + F'_-) = \mu_+ T_+ + (\mu_+ - \kappa) T_- + (F'_+ + F'_-)$$

551
$$= \mu_+ T_s - \kappa T_- + (F'_+ + F'_-) = \mu_+ T_s - \frac{\kappa}{2} (T_s - T_a) + (F'_+ + F'_-)$$

552
$$= \frac{\hat{\lambda}}{2} T_s + \frac{\kappa}{2} T_a + (F'_+ + F'_-) = \frac{\hat{\lambda}}{2} T_s + \frac{\kappa}{2} T_a + F'$$

553
$$\dot{T}_a = \mu_+ T_+ - \mu_- T_- + (F'_+ - F'_-) = \mu_+ T_+ - (\mu_+ - \kappa) T_- + (F'_+ - F'_-)$$

554
$$= \mu_+ T_a + \kappa T_- + (F'_+ - F'_-) = \mu_+ T_a + \frac{\kappa}{2} (T_s - T_a) + (F'_+ - F'_-)$$

555
$$= \frac{\kappa}{2} T_s + \frac{\hat{\lambda}}{2} T_a + (F'_+ - F'_-) = \frac{\kappa}{2} T_s + \frac{\hat{\lambda}}{2} T_a + \frac{\hat{\lambda} + 2\gamma'_d}{\kappa} F' \therefore$$

556
$$N = \frac{1}{2} \left(\hat{\lambda} C_s + \kappa C_a \right) T_s + \frac{1}{2} \left(\hat{\lambda} C_a + \kappa C_s \right) T_a + \left(C_s + C_a \frac{\hat{\lambda} + 2\gamma'_d}{\kappa} \right) F'$$

557

Further expanding the coefficients

$$\hat{\lambda}C_s + \kappa C_a = \hat{\lambda}C_u - \frac{C_d}{2\varepsilon\gamma'}(\hat{\lambda}^2 + 2\gamma'_d\hat{\lambda} - \kappa^2) = \hat{\lambda}C_u - \frac{C_d}{2\varepsilon\gamma'}(\hat{\lambda}^2 + 2\gamma'_d\hat{\lambda} - \hat{\lambda}^2 - 4\gamma'_d\lambda')$$

$$= 2\frac{C_u}{\varepsilon}\left(\lambda' + \frac{\varepsilon-1}{2}\hat{\lambda}\right)$$

$$\hat{\lambda}C_a + \kappa C_s = \kappa C_u - \frac{C_d}{2\varepsilon\gamma'}(\kappa\hat{\lambda} + 2\gamma'_d\kappa - \kappa\hat{\lambda}) = \kappa C_u - \frac{C_u}{\varepsilon}\kappa = \kappa\frac{C_u}{\varepsilon}(\varepsilon-1)$$

$$C_s + C_a\frac{\hat{\lambda} + 2\gamma'_d}{\kappa} = C_u - \frac{C_d}{2\varepsilon\gamma'}(\hat{\lambda} + 2\gamma'_d - \hat{\lambda} - 2\gamma'_d) = C_u$$

then the imbalance is

$$N = \frac{C_u}{\varepsilon}\left[\varepsilon F' + \left(\lambda' + \frac{\varepsilon-1}{2}\hat{\lambda}\right)T_s + \kappa\frac{\varepsilon-1}{2}T_a\right] \quad (\text{A14})$$

From here, I derive the slope of a NT -diagram. In such a diagram, N is plotted versus T_u . If we naively take the partial derivative of equation (A14) with respect to T_u , we will arrive to a constant slope. This is contrary to the evidence that it will change with time. An NT -diagram is one projection of the phase space of the system. Then, the NT -diagram slope does not only depend on how N varies with T_u . It is a comparison of how the changes of T_u are expressed in changes of N . Then, the slope is the total derivative dN/dT_u . By virtue of the chain rule, $dN/dT_u = \dot{N}(dt/dT_u)$. In a neighborhood where $T_u(t)$ is injective, $dt/dT_u = 1/\dot{T}_u$. Therefore, the slope dN/dT_u is the ratio of two total derivatives: \dot{N} and \dot{T}_u .

We know that $T_u = T_s$, then $\dot{T}_u = \dot{T}_s$. Therefore, the total derivative of the planetary imbalance is

$$\dot{N} = (\partial_t N) + (\partial_{T_s} N)\dot{T}_s + (\partial_{T_a} N)\dot{T}_a$$

that is a change depending only on time, a second change depending only on changes of T_s and a third depending on changes of T_a . Therefore, the ratio of total derivative of planetary imbalance and total derivative of T_u is

$$\frac{\dot{N}}{\dot{T}_u} = (\partial_t N)\frac{1}{\dot{T}_s} + (\partial_{T_s} N) + (\partial_{T_a} N)\frac{\dot{T}_a}{\dot{T}_s}$$

583 As one can see in the above expression, the ratio includes the derivative of the imbalance with
584 respect to T_u but is not the only contribution. One contribution comes from the explicit dependence
585 on time of N and how it compares with the dependency of T_u . The other contribution comes
586 from the antisymmetric mode and how it changes in relation to the symmetric one. From equation
587 (A14), I can write the precise expression of the slope as a factor of λ .

588 I multiply equation (A14) by λ/λ and reorganise.

$$589 \quad \frac{\dot{N}}{\dot{T}_u} = \frac{C_u}{\varepsilon} \left[\varepsilon \frac{\dot{F}'}{\dot{T}_s} + \left(\lambda' + \frac{\varepsilon-1}{2} \hat{\lambda} \right) + \kappa \frac{\varepsilon-1}{2} \frac{\dot{T}_a}{\dot{T}_s} \right] \frac{\lambda}{\lambda}$$

$$590 \quad = \left[\frac{C_u \dot{F}'}{\lambda \dot{T}_s} + \left(\frac{\lambda'}{\varepsilon \lambda'} + \frac{\varepsilon-1}{2\varepsilon} \frac{\hat{\lambda}}{\lambda'} \right) + \frac{\varepsilon-1}{2\varepsilon} \frac{\kappa \dot{T}_a}{\lambda' \dot{T}_s} \right] \lambda$$

592 then we will expand the terms to separate the terms that vanish when $\varepsilon = 1$

$$593 \quad \frac{\dot{N}}{\dot{T}_u} = \left\{ \frac{C_u \dot{F}'}{\lambda \dot{T}_s} + \left[\frac{1}{\varepsilon} + \frac{\varepsilon-1}{2\varepsilon} \left(\frac{\lambda' - \varepsilon \gamma' - \gamma'_d}{\lambda'} \right) \right] + \frac{\varepsilon-1}{2\varepsilon} \frac{\kappa \dot{T}_a}{\lambda' \dot{T}_s} \right\} \lambda$$

$$594 \quad = \left\{ \frac{C_u \dot{F}'}{\lambda \dot{T}_s} + \left[\frac{2}{2\varepsilon} + \frac{\varepsilon-1}{2\varepsilon} \left(1 - \varepsilon \frac{\gamma}{\lambda} - \frac{C_u \gamma}{C_d \lambda} \right) \right] + \frac{\varepsilon-1}{2\varepsilon} \frac{C_u \kappa \dot{T}_a}{\lambda \dot{T}_s} \right\} \lambda$$

$$595 \quad = \left[\frac{C_u \dot{F}'}{\lambda \dot{T}_s} + \frac{\varepsilon+1}{2\varepsilon} - \frac{\varepsilon-1}{2\varepsilon} \left(\varepsilon + \frac{C_u}{C_d} \right) \frac{\gamma}{\lambda} + \frac{\varepsilon-1}{2\varepsilon} \frac{C_u \kappa \dot{T}_a}{\lambda \dot{T}_s} \right] \lambda$$

$$596 \quad = \left[\frac{C_u \dot{F}'}{\lambda \dot{T}_s} + \frac{\varepsilon+1}{2\varepsilon} - \frac{\varepsilon-1}{2\varepsilon} \left(\varepsilon + \frac{C_u}{C_d} \right) \frac{\gamma}{\lambda} + \frac{\varepsilon-1}{2\varepsilon} \frac{C_u \kappa \dot{T}_a}{\lambda \dot{T}_s} \right] \lambda$$

$$597 \quad = \left\{ \frac{C_u \dot{F}'}{\lambda \dot{T}_s} + \frac{\varepsilon+1}{2\varepsilon} - \frac{\varepsilon-1}{2\varepsilon \lambda} \left[\left(\varepsilon + \frac{C_u}{C_d} \right) \gamma - C_u \kappa \frac{\dot{T}_a}{\dot{T}_s} \right] \right\} \lambda$$

$$598 \quad = \left\{ \frac{C_u \dot{F}'}{\lambda \dot{T}_s} + \frac{\varepsilon+1}{2\varepsilon} - \frac{\varepsilon-1}{2\varepsilon \lambda} C_u \kappa \left[\left(\varepsilon + \frac{C_u}{C_d} \right) \frac{\gamma}{C_u \kappa} - \frac{\dot{T}_a}{\dot{T}_s} \right] \right\} \lambda$$

$$599 \quad = \left\{ \frac{C_u \dot{F}'}{\lambda \dot{T}_s} + \frac{\varepsilon+1}{2\varepsilon} - \frac{\varepsilon-1}{2\varepsilon} \frac{C_u \kappa}{\lambda} \left[\left(\varepsilon + \frac{C_u}{C_d} \right) \frac{\gamma}{C_u \kappa} - \frac{\dot{T}_a}{\dot{T}_s} \right] \right\} \lambda$$

$$600 \quad = \left\{ -\frac{C_u \dot{F}'}{|\lambda| \dot{T}_s} + \frac{\varepsilon+1}{2\varepsilon} + \frac{\varepsilon-1}{2\varepsilon} \frac{C_u \kappa}{|\lambda|} \left[\left(\varepsilon + \frac{C_u}{C_d} \right) \frac{\gamma}{C_u \kappa} - \frac{\dot{T}_a}{\dot{T}_s} \right] \right\} \lambda$$

$$601$$

$$602$$

$$603 \quad \frac{\dot{N}}{\dot{T}_u} = \left\{ -\frac{C_u \dot{F}'}{|\lambda| \dot{T}_s} + \frac{\varepsilon+1}{2\varepsilon} \left(1 + \frac{\varepsilon-1}{\varepsilon+1} \frac{C_u \kappa}{|\lambda|} \left[\left(\varepsilon + \frac{C_u}{C_d} \right) \frac{\gamma}{C_u \kappa} - \frac{\dot{T}_a}{\dot{T}_s} \right] \right) \right\} \lambda \quad (A15)$$

$$604$$

605 The term in square brackets in equation (A15) is the key term that provides a NT -diagram with
606 evolving slope when the forcing is constant. The second part of this term provides the temporal

607 evolution, whereas the first part is a constant term that sets the base enhancement of the slope.
 608 Interestingly, this first part contains in particular the thermal capacities of the system.

609 If I rewrite this first part of the square-brackets term, the terms are shown clearly

$$610 \quad \frac{\dot{N}}{\dot{T}_u} = \left\{ -\frac{C_u \dot{F}'}{|\lambda| \dot{T}_s} + \frac{\varepsilon + 1}{2\varepsilon} + \frac{\varepsilon - 1}{2\varepsilon} \frac{C_u \kappa}{|\lambda|} \left[\left(\frac{\varepsilon}{C_u} + \frac{1}{C_d} \right) \frac{\gamma}{\kappa} - \frac{\dot{T}_a}{\dot{T}_s} \right] \right\} \lambda \quad (A16)$$

611

612 Now in the first part it is the sum of the inverse of the thermal capacities as if we have an electrical
 613 circuit with capacitors in series. Having such a term in the equation for the slope favors the physical
 614 interpretation in terms of thermal capacities, instead of variable feedback mechanisms. The time-
 615 evolving ratio term in the second part, that represents the dynamics of the atmosphere-ocean
 616 coupling, only strengthens this interpretation.

617 As a corollary, if the forcing is constant and $\varepsilon \rightarrow 1$, then we recover the classical linear dependence
 618 of the imbalance on T_u

$$619 \quad \lim_{\varepsilon \rightarrow 1} \frac{\dot{N}}{\dot{T}_u} = \lambda, F = \text{const}$$

620

621 **Symmetric and antisymmetric modes**

622 From equations (A13), we see that the symmetric and antisymmetric modes are the basis for
 623 the description of the solutions. Thus, let us give some explicit expression for the symmetric and
 624 antisymmetric modes.

625 From equation (A12) and the equations for the initial values and the forcing, I can write more
 626 explicitly the solution

$$\begin{aligned}
 627 \quad T_{\pm} &= \left(T_{\pm,0} + \int_{t_0}^t F'_{\pm} e^{-\mu_{\pm}(\tau-t_0)} d\tau \right) e^{\mu_{\pm}(t-t_0)} \\
 628 \quad &= \left(\pm \frac{1}{\mu_+ - \mu_-} [(\mu_{\pm} + \gamma'_d)T_{u,0} + \varepsilon\gamma'T_{d,0}] \pm \frac{\mu_{\pm} + \gamma'_d}{\mu_+ - \mu_-} \int_{t_0}^t F' e^{-\mu_{\pm}(\tau-t_0)} d\tau \right) e^{\mu_{\pm}(t-t_0)} \\
 629 \quad &= \pm \frac{e^{(\hat{\lambda}/2)(t-t_0)}}{\mu_+ - \mu_-} \left[(\mu_{\pm} + \gamma'_d)T_{u,0} + \varepsilon\gamma'T_{d,0} + (\mu_{\pm} + \gamma'_d) \int_{t_0}^t F' e^{-\mu_{\pm}(\tau-t_0)} d\tau \right] e^{\pm(\kappa/2)(t-t_0)} \\
 630 \quad &= \pm \frac{e^{(\hat{\lambda}/2)(t-t_0)}}{\mu_+ - \mu_-} \left[\frac{\hat{\lambda} \pm \kappa + 2\gamma'_d}{2} T_{u,0} + \frac{2\varepsilon\gamma'}{2} T_{d,0} + \frac{\hat{\lambda} \pm \kappa + 2\gamma'_d}{2} \int_{t_0}^t F' e^{-\mu_{\pm}(\tau-t_0)} d\tau \right] e^{\pm(\kappa/2)(t-t_0)} \\
 631 \quad &= \pm \frac{e^{(\hat{\lambda}/2)(t-t_0)}}{2(\mu_+ - \mu_-)} \left[(\hat{\lambda} + 2\gamma'_d)T_{u,0} + 2\varepsilon\gamma'T_{d,0} \pm \kappa T_{u,0} + (\hat{\lambda} + 2\gamma'_d \pm \kappa) \int_{t_0}^t F' e^{-\mu_{\pm}(\tau-t_0)} d\tau \right] e^{\pm(\kappa/2)(t-t_0)} \\
 632
 \end{aligned}$$

633 Now that I have a more explicit expression, I write the modes

$$\begin{aligned}
 634 \quad & T_+ \pm T_- = \\
 635 \quad & \frac{e^{(\hat{\lambda}/2)(t-t_0)}}{2(\mu_+ - \mu_-)} \left[(\hat{\lambda} + 2\gamma'_d)T_{u,0} + 2\varepsilon\gamma'T_{d,0} + \kappa T_{u,0} + (\hat{\lambda} + 2\gamma'_d + \kappa) \int_{t_0}^t F' e^{-\mu_+(\tau-t_0)} d\tau \right] e^{(\kappa/2)(t-t_0)} \\
 636 \quad & \mp \frac{e^{(\hat{\lambda}/2)(t-t_0)}}{2(\mu_+ - \mu_-)} \left[(\hat{\lambda} + 2\gamma'_d)T_{u,0} + 2\varepsilon\gamma'T_{d,0} - \kappa T_{u,0} + (\hat{\lambda} + 2\gamma'_d - \kappa) \int_{t_0}^t F' e^{-\mu_-(\tau-t_0)} d\tau \right] e^{-(\kappa/2)(t-t_0)} \\
 637 \quad & = \frac{e^{(\hat{\lambda}/2)(t-t_0)}}{\mu_+ - \mu_-} \left\{ [(\hat{\lambda} + 2\gamma'_d)T_{u,0} + 2\varepsilon\gamma'T_{d,0}] \frac{e^{(\kappa/2)(t-t_0)} \mp e^{-(\kappa/2)(t-t_0)}}{2} \right. \\
 638 \quad & \quad \left. + \kappa T_{u,0} \frac{e^{(\kappa/2)(t-t_0)} \pm e^{-(\kappa/2)(t-t_0)}}{2} \right. \\
 639 \quad & \quad \left. + \frac{\hat{\lambda} + 2\gamma'_d}{2} \left[e^{(\kappa/2)(t-t_0)} \int_{t_0}^t F' e^{-\mu_+(\tau-t_0)} d\tau \mp e^{-(\kappa/2)(t-t_0)} \int_{t_0}^t F' e^{-\mu_-(\tau-t_0)} d\tau \right] \right. \\
 640 \quad & \quad \left. + \frac{\kappa}{2} \left[e^{(\kappa/2)(t-t_0)} \int_{t_0}^t F' e^{-\mu_+(\tau-t_0)} d\tau \pm e^{-(\kappa/2)(t-t_0)} \int_{t_0}^t F' e^{-\mu_-(\tau-t_0)} d\tau \right] \right\} \\
 641
 \end{aligned}$$

642 The last two terms inside the curly brackets have a similar form as the combinations of exponential
 643 functions in the first two terms. These combinations of exponential functions are hyperbolic
 644 functions which can simplify the expressions of the solutions. I would want such a representation
 645 but a problem is there: the integrals are not the same, therefore I cannot factorise them together.
 646 Notwithstanding, from the definition of hyperbolic sine and cosine functions, I can write $e^{\pm x} =$

647 $\cosh x \pm \sinh x$. The factors within square brackets in the last two terms can be thought as $e^x I_+ \pm$
648 $e^{-x} I_-$, where I_{\pm} are the corresponding integrals. Using the expression of the exponential function in
649 terms of the hyperbolic functions, I expand $e^x I_+ \pm e^{-x} I_- = (\cosh x + \sinh x) I_+ \pm (\cosh x - \sinh x) I_- =$
650 $(I_+ \pm I_-) \cosh x + (I_+ \mp I_-) \sinh x$. Then, I overcome the limitation and now the two terms are written
651 with hyperbolic functions. The coefficients of the hyperbolic functions are simple combinations
652 of the integrals which can be also expanded easily. I do that now

$$\begin{aligned}
653 \quad I_+ + I_- &= \int_{t_0}^t F' e^{-\mu_+(\tau-t_0)} d\tau + \int_{t_0}^t F' e^{-\mu_-(\tau-t_0)} d\tau = \int_{t_0}^t F' [e^{-\mu_+(\tau-t_0)} + e^{-\mu_-(\tau-t_0)}] d\tau \\
654 \quad &= \int_{t_0}^t F' e^{-(\hat{\lambda}/2)(\tau-t_0)} [e^{-(\kappa/2)(\tau-t_0)} + e^{(\kappa/2)(\tau-t_0)}] d\tau \\
655 \quad &= 2 \int_{t_0}^t F' e^{-(\hat{\lambda}/2)(\tau-t_0)} \cosh \left[\frac{\kappa}{2}(\tau-t_0) \right] d\tau \\
656 \quad I_+ - I_- &= \int_{t_0}^t F' e^{-\mu_+(\tau-t_0)} d\tau - \int_{t_0}^t F' e^{-\mu_-(\tau-t_0)} d\tau = \int_{t_0}^t F' [e^{-\mu_+(\tau-t_0)} - e^{-\mu_-(\tau-t_0)}] d\tau \\
657 \quad &= \int_{t_0}^t F' e^{-(\hat{\lambda}/2)(\tau-t_0)} [e^{-(\kappa/2)(\tau-t_0)} - e^{(\kappa/2)(\tau-t_0)}] d\tau \\
658 \quad &= -2 \int_{t_0}^t F' e^{-(\hat{\lambda}/2)(\tau-t_0)} \sinh \left[\frac{\kappa}{2}(\tau-t_0) \right] d\tau \\
659
\end{aligned}$$

660 If one collects terms corresponding to each hyperbolic function in the former expressions for the
661 normal modes, obtains the following

$$662 \quad T_s = \frac{e^{(\hat{\lambda}/2)(t-t_0)}}{\kappa} \left\{ C_1 \cosh \left[\frac{\kappa}{2}(t-t_0) \right] + C_2 \sinh \left[\frac{\kappa}{2}(t-t_0) \right] \right\} \quad (\text{A17})$$

$$663 \quad T_a = \frac{e^{(\hat{\lambda}/2)(t-t_0)}}{\kappa} \left\{ C_2 \cosh \left[\frac{\kappa}{2}(t-t_0) \right] + C_1 \sinh \left[\frac{\kappa}{2}(t-t_0) \right] \right\} \quad (\text{A18})$$

665 where

$$666 \quad C_1 = \kappa T_{u,0}$$

$$667 \quad -(\hat{\lambda} + 2\gamma'_d) \int_{t_0}^t F' e^{-(\hat{\lambda}/2)(\tau-t_0)} \sinh \left[\frac{\kappa}{2}(\tau-t_0) \right] d\tau + \kappa \int_{t_0}^t F' e^{-(\hat{\lambda}/2)(\tau-t_0)} \cosh \left[\frac{\kappa}{2}(\tau-t_0) \right] d\tau$$

$$668 \quad C_2 = (\hat{\lambda} + 2\gamma'_d) T_{u,0} + 2\varepsilon\gamma'_d T_{d,0}$$

$$669 \quad + (\hat{\lambda} + 2\gamma'_d) \int_{t_0}^t F' e^{-(\hat{\lambda}/2)(\tau-t_0)} \cosh \left[\frac{\kappa}{2}(\tau-t_0) \right] d\tau - \kappa \int_{t_0}^t F' e^{-(\hat{\lambda}/2)(\tau-t_0)} \sinh \left[\frac{\kappa}{2}(\tau-t_0) \right] d\tau$$

671 These expressions for the normal modes are quite elegant, and the coefficients C_i summarize
672 all the information from the initial conditions and the forcing. The initial condition terms in the
673 C_i correspond to the non-forced response of the system, while the part that is forcing-dependent
674 corresponds to the forced response of the system.

675 **Forced response to constant forcing**

676 If $F' = F'_c \neq 0$ for $t > t_0$ with F'_c constant and $T_{u,0}, T_{d,0} = 0$ for $t = t_0$, then

$$677 \quad C_1 = F'_c \left\{ -(\hat{\lambda} + 2\gamma'_d) \int_{t_0}^t e^{-(\hat{\lambda}/2)(\tau-t_0)} \sinh \left[\frac{\kappa}{2}(\tau-t_0) \right] d\tau + \kappa \int_{t_0}^t e^{-(\hat{\lambda}/2)(\tau-t_0)} \cosh \left[\frac{\kappa}{2}(\tau-t_0) \right] d\tau \right\}$$

$$678 \quad C_2 = F'_c \left\{ (\hat{\lambda} + 2\gamma'_d) \int_{t_0}^t e^{-(\hat{\lambda}/2)(\tau-t_0)} \cosh \left[\frac{\kappa}{2}(\tau-t_0) \right] d\tau - \kappa \int_{t_0}^t e^{-(\hat{\lambda}/2)(\tau-t_0)} \sinh \left[\frac{\kappa}{2}(\tau-t_0) \right] d\tau \right\}$$

680 where the integrals are easily computed

$$681 \quad \int_{t_0}^t e^{-(\hat{\lambda}/2)(\tau-t_0)} \sinh \left[\frac{\kappa}{2}(\tau-t_0) \right] d\tau = \frac{e^{-(\hat{\lambda}/2)(t-t_0)}}{\lambda'\gamma'_d} \left\{ \frac{\kappa}{2} \cosh \left[\frac{\kappa}{2}(t-t_0) \right] + \frac{\hat{\lambda}}{2} \sinh \left[\frac{\kappa}{2}(t-t_0) \right] \right\} - \frac{\kappa}{2\lambda'\gamma'_d}$$

$$682 \quad \int_{t_0}^t e^{-(\hat{\lambda}/2)(\tau-t_0)} \cosh \left[\frac{\kappa}{2}(\tau-t_0) \right] d\tau = \frac{e^{-(\hat{\lambda}/2)(t-t_0)}}{\lambda'\gamma'_d} \left\{ \frac{\hat{\lambda}}{2} \cosh \left[\frac{\kappa}{2}(t-t_0) \right] + \frac{\kappa}{2} \sinh \left[\frac{\kappa}{2}(t-t_0) \right] \right\} - \frac{\hat{\lambda}}{2\lambda'\gamma'_d}$$

684 and, upon reduction, the C_i are

$$685 \quad C_1 = \frac{F'_c}{\lambda'} e^{-(\hat{\lambda}/2)(\tau-t_0)} \left\{ -\kappa \cosh \left[\frac{\kappa}{2}(t-t_0) \right] + (2\lambda' - \hat{\lambda}) \sinh \left[\frac{\kappa}{2}(t-t_0) \right] + \kappa e^{(\hat{\lambda}/2)(t-t_0)} \right\}$$

$$686 \quad C_2 = \frac{F'_c}{\lambda'} e^{-(\hat{\lambda}/2)(\tau-t_0)} \left\{ -(2\lambda' - \hat{\lambda}) \cosh \left[\frac{\kappa}{2}(t-t_0) \right] + \kappa \sinh \left[\frac{\kappa}{2}(t-t_0) \right] + (2\lambda' - \hat{\lambda}) e^{(\hat{\lambda}/2)(t-t_0)} \right\}$$

687

688 with these expressions is easy to evaluate the terms inside the curly brackets in equations (A17)
689 and (A18) and the symmetric and antisymmetric modes are (for $t \geq t_0$)

$$690 \quad T_s = \frac{F_c}{\lambda} \left\{ e^{(\hat{\lambda}/2)(t-t_0)} \left(\cosh \left[\frac{\kappa}{2}(t-t_0) \right] + \frac{2\lambda' - \hat{\lambda}}{\kappa} \sinh \left[\frac{\kappa}{2}(t-t_0) \right] \right) - 1 \right\} \quad (\text{A19})$$

$$691 \quad T_a = \frac{F_c}{\lambda} \left\{ e^{(\hat{\lambda}/2)(t-t_0)} \left(\frac{2\lambda' - \hat{\lambda}}{\kappa} \cosh \left[\frac{\kappa}{2}(t-t_0) \right] + \sinh \left[\frac{\kappa}{2}(t-t_0) \right] \right) - \frac{2\lambda' - \hat{\lambda}}{\kappa} \right\} \quad (\text{A20})$$

693 where $F'_c := F_c/C_u$. I can also obtain the explicit time derivatives of both modes. We take the time
694 derivative both equations (A19) and (A20)

$$695 \quad \begin{aligned} \dot{T}_s &= \frac{F_c}{\lambda} e^{(\hat{\lambda}/2)(t-t_0)} \left\{ \hat{\lambda} \left(\cosh \left[\frac{\kappa}{2}(t-t_0) \right] + \frac{2\lambda' - \hat{\lambda}}{\kappa} \sinh \left[\frac{\kappa}{2}(t-t_0) \right] \right) \right. \\ &\quad \left. + \frac{\kappa}{2} \left(\frac{2\lambda' - \hat{\lambda}}{\kappa} \cosh \left[\frac{\kappa}{2}(t-t_0) \right] + \sinh \left[\frac{\kappa}{2}(t-t_0) \right] \right) \right\} \\ 696 &= \frac{F_c}{\lambda} e^{(\hat{\lambda}/2)(t-t_0)} \left\{ \lambda' \cosh \left[\frac{\kappa}{2}(t-t_0) \right] + \frac{\lambda' \hat{\lambda} + 2\gamma'_d \lambda'}{\kappa} \sinh \left[\frac{\kappa}{2}(t-t_0) \right] \right\} \\ 697 &= \frac{F_c}{C_u} e^{(\hat{\lambda}/2)(t-t_0)} \left\{ \cosh \left[\frac{\kappa}{2}(t-t_0) \right] + \frac{\hat{\lambda} + 2\gamma'_d}{\kappa} \sinh \left[\frac{\kappa}{2}(t-t_0) \right] \right\} \\ 698 & \\ \dot{T}_a &= \frac{F_c}{\lambda} e^{(\hat{\lambda}/2)(t-t_0)} \left\{ \hat{\lambda} \left(\frac{2\lambda' - \hat{\lambda}}{\kappa} \cosh \left[\frac{\kappa}{2}(t-t_0) \right] + \sinh \left[\frac{\kappa}{2}(t-t_0) \right] \right) \right. \\ 699 &\quad \left. + \frac{\kappa}{2} \left(\cosh \left[\frac{\kappa}{2}(t-t_0) \right] + \frac{2\lambda' - \hat{\lambda}}{\kappa} \sinh \left[\frac{\kappa}{2}(t-t_0) \right] \right) \right\} \\ 700 &= \frac{F_c}{\lambda} e^{(\hat{\lambda}/2)(t-t_0)} \left\{ \frac{\lambda' \hat{\lambda} + 2\gamma'_d \lambda'}{\kappa} \cosh \left[\frac{\kappa}{2}(t-t_0) \right] + \lambda' \sinh \left[\frac{\kappa}{2}(t-t_0) \right] \right\} \\ 701 &= \frac{F_c}{C_u} e^{(\hat{\lambda}/2)(t-t_0)} \left\{ \frac{\hat{\lambda} + 2\gamma'_d}{\kappa} \cosh \left[\frac{\kappa}{2}(t-t_0) \right] + \sinh \left[\frac{\kappa}{2}(t-t_0) \right] \right\} \\ 702 & \\ 703 & \end{aligned}$$

704 I present both results jointly to show the simplicity of the derivatives

$$705 \quad \begin{aligned} \dot{T}_s &= \frac{F_c}{C_u} e^{(\hat{\lambda}/2)(t-t_0)} \left\{ \cosh \left[\frac{\kappa}{2}(t-t_0) \right] + \frac{\hat{\lambda} + 2\gamma'_d}{\kappa} \sinh \left[\frac{\kappa}{2}(t-t_0) \right] \right\} \\ 706 \quad \dot{T}_a &= \frac{F_c}{C_u} e^{(\hat{\lambda}/2)(t-t_0)} \left\{ \frac{\hat{\lambda} + 2\gamma'_d}{\kappa} \cosh \left[\frac{\kappa}{2}(t-t_0) \right] + \sinh \left[\frac{\kappa}{2}(t-t_0) \right] \right\} \\ 707 & \end{aligned}$$

708 With these derivatives, I can calculate the ratio of the antisymmetric mode derivative to the
 709 symmetric one that appears in equation (A15)

$$\begin{aligned}
 \frac{\dot{T}_a}{\dot{T}_s} &= \frac{\frac{\hat{\lambda}+2\gamma'_d}{\kappa} \cosh\left[\frac{\kappa}{2}(t-t_0)\right] + \sinh\left[\frac{\kappa}{2}(t-t_0)\right]}{\cosh\left[\frac{\kappa}{2}(t-t_0)\right] + \frac{\hat{\lambda}+2\gamma'_d}{\kappa} \sinh\left[\frac{\kappa}{2}(t-t_0)\right]} \\
 &= \frac{\frac{\hat{\lambda}+2\gamma'_d}{\kappa} + \tanh\left[\frac{\kappa}{2}(t-t_0)\right]}{1 + \frac{\hat{\lambda}+2\gamma'_d}{\kappa} \tanh\left[\frac{\kappa}{2}(t-t_0)\right]}
 \end{aligned}$$

713 Formally, above result have the alternative form

$$\frac{\dot{T}_a}{\dot{T}_s} = \tanh\left[\frac{\kappa}{2}(t-t_0) + \operatorname{arctanh}\left(\frac{\hat{\lambda}+2\gamma'_d}{\kappa}\right)\right]$$

716 This is possible only if $|(\hat{\lambda}+2\gamma'_d)/\kappa| \leq 1$. Let us prove that in our case this follows

$$\begin{aligned}
 \left|\frac{\hat{\lambda}+2\gamma'_d}{\kappa}\right| &\leq 1 \\
 \frac{\hat{\lambda}^2 + 4\gamma'_d\hat{\lambda} + 4\gamma'^2_d}{\hat{\lambda}^2 + 4\gamma'_d\lambda'} &\leq 1 \\
 \hat{\lambda}^2 + 4\gamma'_d\hat{\lambda} + 4\gamma'^2_d &\leq \hat{\lambda}^2 + 4\gamma'_d\lambda' \\
 \hat{\lambda} + \gamma'_d &\leq \lambda' \\
 -\varepsilon\gamma' &\leq 0
 \end{aligned}$$

723 the last inequality is always true, since ε, γ' are positive constants. Thus,

$$\frac{\dot{T}_a}{\dot{T}_s} = \tanh\left[\frac{\kappa}{2}(t-t_0) + \operatorname{arctanh}\left(\frac{\hat{\lambda}+2\gamma'_d}{\kappa}\right)\right] \tag{A21}$$

726 Equation (A21) is an hyperbolic tangent that grows from -1 to 1 in a sigmoidal fashion. It has a
 727 scaling factor that determines how fast it goes from -1 to 1. It also has a shift that sets where the
 728 hyperbolic tangent will cross zero. Both the scaling and shift depend on the thermal and radiative
 729 parameters of the system. Since the shift is negative, after the initial forcing the deep ocean (that
 730 depends on the antisymmetric mode) warms up slower than the upper ocean. At a latter time, the

731 ratio becomes positive and the contrary happens. The time at which the sign reverses is

$$732 \quad t_1 = t_0 + \frac{2}{\kappa} \operatorname{arctanh} \left| \frac{\hat{\lambda} + 2\gamma'_d}{\kappa} \right|$$

733

734 **Variation of the climate feedback parameter**

735 With the solution shown before, the NT -diagram has a slope

$$736 \quad \frac{\dot{N}}{\dot{T}_u} = \frac{\varepsilon + 1}{2\varepsilon} \left(1 + \frac{\varepsilon - 1}{\varepsilon + 1} \frac{C_u \kappa}{|\lambda|} \left[\left(\varepsilon + \frac{C_u}{C_d} \right) \frac{\gamma}{C_u \kappa} - \tanh \left(\frac{\kappa}{2} (t - t_0) + \operatorname{arctanh} \left(\frac{\hat{\lambda} + 2\gamma'_d}{\kappa} \right) \right) \right] \right) \lambda \quad (\text{A22})$$

737

738 The factor is composed of terms that are positive except for the ratio term coming from equation
 739 (A21). The negative ratio for $t \in [t_0, t_1)$ clearly generates a more negative slope, whereas for
 740 $t \in (t_1, \infty)$ makes it less negative. At the start one can get the slope

$$741 \quad \frac{\dot{N}}{\dot{T}_u} = \left(1 + (\varepsilon - 1) \frac{\gamma}{|\lambda|} \right) \lambda, t = t_0$$

742

743 and at the time of sign reversal

$$744 \quad \frac{\dot{N}}{\dot{T}_u} = \frac{\varepsilon + 1}{2\varepsilon} \left(1 + \frac{\varepsilon - 1}{\varepsilon + 1} \left(\varepsilon + \frac{C_u}{C_d} \right) \frac{\gamma}{|\lambda|} \right) \lambda, t = t_1$$

745

746 After the sign reversal the factor of λ will only decrease up to

$$747 \quad \lim_{t \rightarrow \infty} \frac{\dot{N}}{\dot{T}_u} = \frac{\varepsilon + 1}{2\varepsilon} \left(1 + \frac{\varepsilon - 1}{\varepsilon + 1} \frac{C_u \kappa}{|\lambda|} \left[\left(\varepsilon + \frac{C_u}{C_d} \right) \frac{\gamma}{C_u \kappa} - 1 \right] \right) \lambda$$

748

749 Equation (A22) shows the importance of the ratio of the symmetric and antisymmetric modes. Its
 750 physical meaning, the relationship between the upper- and deep-ocean warming, sets the strength
 751 of the variation of the climate feedback, whereas the constant term sets a base enhancement around
 752 which the feedback evolves. The thermal capacities of the system determine this constant term.

References

Andrews, T., J. M. Gregory, M. J. Webb, and K. E. Taylor, 2012: Forcing, feedbacks and climate sensitivity in CMIP5 coupled atmosphere-ocean climate models. *Geophys. Res. Lett.*, **39** (9), L09 712, doi:10.1029/2012GL051607.

Armour, K. C., C. M. Bitz, and G. H. Roe, 2013: Time-Varying Climate Sensitivity from Regional Feedbacks. *J. Climate*, **26** (13), 4518–4534, doi:10.1175/JCLI-D-12-00544.1.

Ceppi, P., and J. M. Gregory, 2017: Relationship of tropospheric stability to climate sensitivity and Earth’s observed radiation budget. *Proc. Natl. Acad. Sci. (USA)*, **114** (50), 13 126–13 131, doi:10.1073/pnas.1714308114.

Geoffroy, O., D. Saint-Martin, G. Bellon, A. Voldoire, D. J. L. Olivié, and S. Tytéca, 2013a: Transient Climate Response in a Two-Layer Energy-Balance Model. Part II: Representation of the Efficacy of Deep-Ocean Heat Uptake and Validation for CMIP5 AOGCMs. *J. Climate*, **26** (6), 1859–1876, doi:10.1175/JCLI-D-12-00196.1.

Geoffroy, O., D. Saint-Martin, D. J. L. Olivié, A. Voldoire, G. Bellon, and S. Tytéca, 2013b: Transient Climate Response in a Two-Layer Energy-Balance Model. Part I: Analytical Solution and Parameter Calibration Using CMIP5 AOGCM Experiments. *J. Climate*, **26** (6), 1841–1857, doi:10.1175/JCLI-D-12-00195.1.

Gregory, J. M., R. J. Stouffer, S. C. B. Raper, P. A. Stott, and N. A. Rayner, 2002: An Observationally Based Estimate of the Climate Sensitivity. *J. Climate*, **15** (22), 3117–3121, doi:10.1175/1520-0442(2002)015<3117:AOBEOT>2.0.CO;2.

- 773 Grose, M. R., J. Gregory, R. Colman, and T. Andrews, 2018: What Climate Sensitiv-
774 ity Index Is Most Useful for Projections? *Geophys. Res. Lett.*, **45** (3), 1559–1566, doi:
775 10.1002/2017GL075742.
- 776 Hawkins, E., and R. Sutton, 2009: The Potential to Narrow Uncertainty in Regional Climate
777 Predictions. *Bull. Amer. Meteor. Soc.*, **90** (8), 1095–1107, doi:10.1175/2009BAMS2607.1.
- 778 Held, I. M., M. Winton, K. Takahashi, T. Delworth, F. Zeng, and G. K. Vallis, 2010: Probing the
779 Fast and Slow Components of Global Warming by Returning Abruptly to Preindustrial Forcing.
780 *J. Climate*, **23** (9), 2418–2427, doi:10.1175/2009JCLI3466.1.
- 781 Jiménez-de-la-Cuesta, D., and T. Mauritsen, 2019: Emergent constraints on Earth’s transient and
782 equilibrium response to doubled CO₂ from post-1970s warming. *Nat. Geosci.*, **12** (11), 902–905,
783 doi:10.1038/s41561-019-0463-y.
- 784 Kiehl, J., 2007: Twentieth century climate model response and climate sensitivity. *Geophys. Res.*
785 *Lett.*, **34** (22), L22 710, doi:10.1029/2007GL031383.
- 786 Mauritsen, T., 2016: Clouds cooled the Earth. *Nat. Geosci.*, **9** (12), 865–867, doi:10.1038/
787 ngeo2838.
- 788 Meraner, K., T. Mauritsen, and A. Voigt, 2013: Robust increase in equilibrium climate sensitivity
789 under global warming. *Geophys. Res. Lett.*, **40** (2), 5944–5948, doi:10.1002/2013GL058118.
- 790 Rohrschneider, T., B. Stevens, and T. Mauritsen, 2019: On simple representations of the
791 climate response to external radiative forcing. *Climate Dyn.*, **3** (5-6), 3131–3145, doi:
792 10.1007/s00382-019-04686-4.
- 793 Senior, C. A., and J. F. B. Mitchell, 2000: The time-dependence of climate sensitivity. *Geophys.*
794 *Res. Lett.*, **27** (17), 2685–2688, doi:10.1029/2000GL011373.

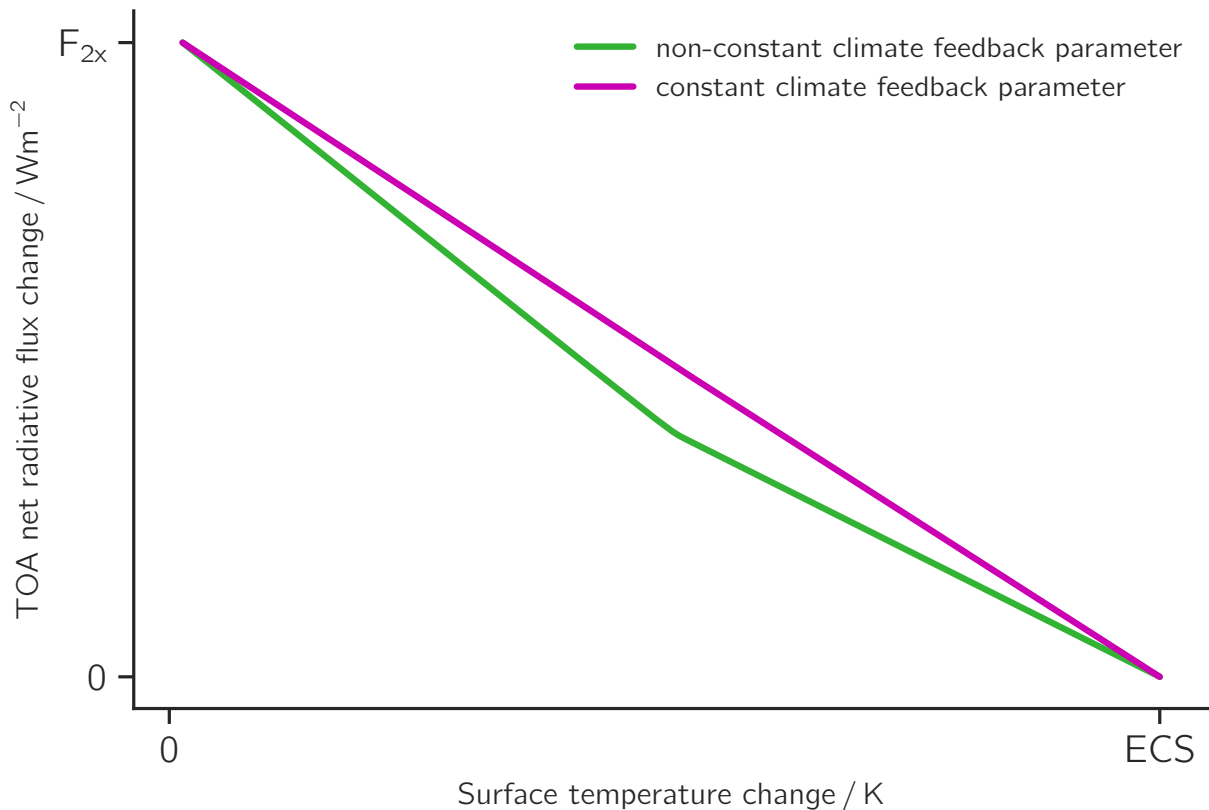
- 795 Stevens, B., S. C. Sherwood, S. Bony, and M. J. Webb, 2016: Prospects for narrowing
796 bounds on Earth's equilibrium climate sensitivity. *Earths Future*, **4** (11), 512–522, doi:
797 10.1002/2016EF000376.
- 798 Winton, M., K. Takahashi, and I. M. Held, 2010: Importance of Ocean Heat Uptake Efficacy to
799 Transient Climate Change. *J. Climate*, **23** (9), 2333–2344, doi:10.1175/2009JCLI3139.1.
- 800 Zhou, C., M. D. Zelinka, and S. A. Klein, 2016: Impact of decadal cloud variations on the Earth's
801 energy budget. *Nat. Geosci.*, **9** (12), 871–874, doi:10.1038/ngeo2828.

802 **LIST OF FIGURES**

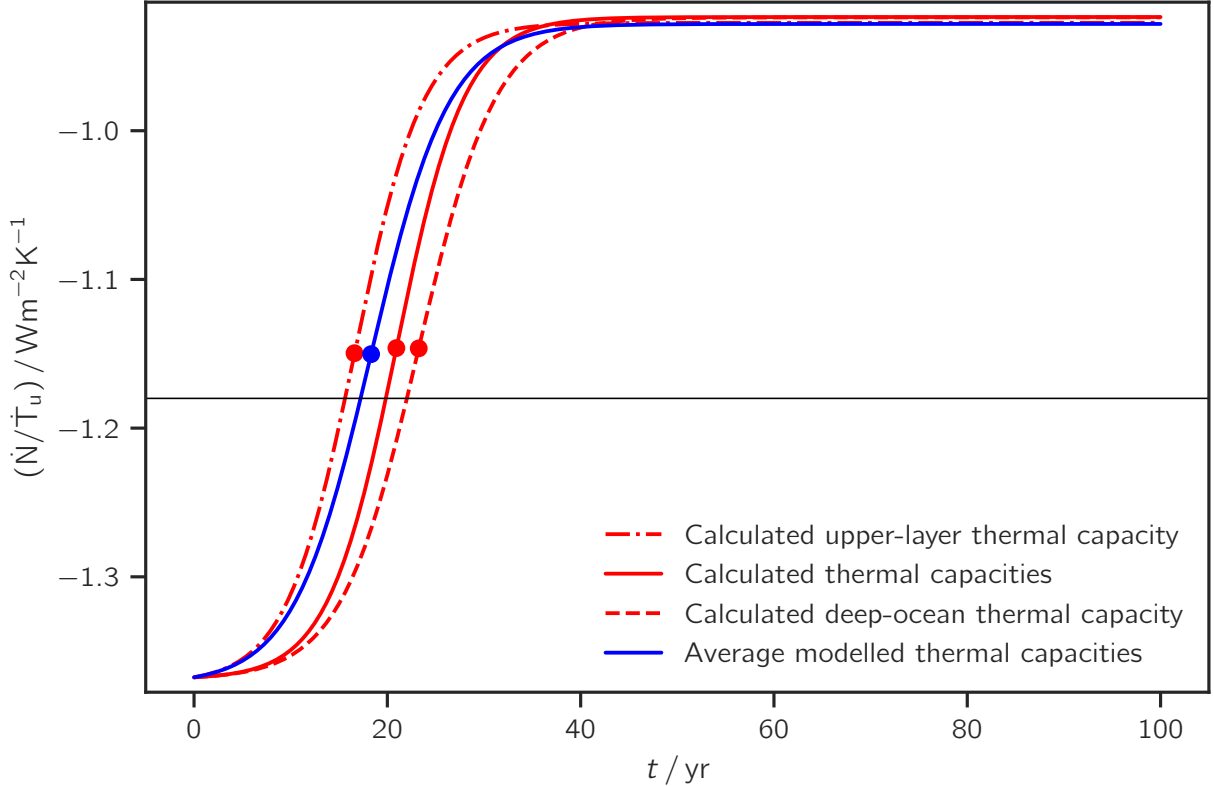
803 **Fig. 1.** Schematic representation of an NT -diagram for constant forcing due to a doubling of the
804 atmospheric carbon dioxide concentration (F_{2x}). Magenta line represents the relationship
805 between the TOA net radiative flux change with the surface temperature change if the
806 feedback mechanisms on surface warming were constant (constant slope). Green line shows
807 the case found in most models, where the slope varies throughout the process. Given that most
808 models are not run until equilibrium, the evolving slope introduces considerable uncertainty
809 in the equilibrium climate sensitivity (ECS) estimates 40

810 **Fig. 2.** Evolution of the slope of an NT -diagram. Blue solid line, with the average parameters
811 from CMIP5 models obtained by Geoffroy et al. (2013a). Red solid line, with the thermal
812 capacities as calculated by Jiménez-de-la-Cuesta and Mauritsen (2019). Red dashed line,
813 with C_d as in Jiménez-de-la-Cuesta and Mauritsen (2019). Red dash-dotted line, with C_u as
814 in Jiménez-de-la-Cuesta and Mauritsen (2019). Dots represent the slope values when the
815 ratio term \dot{T}_a/\dot{T}_s has the sign reversal. Thin black line is the constant $\lambda = -1.18 \text{ W m}^{-2} \text{ K}^{-1}$ 41

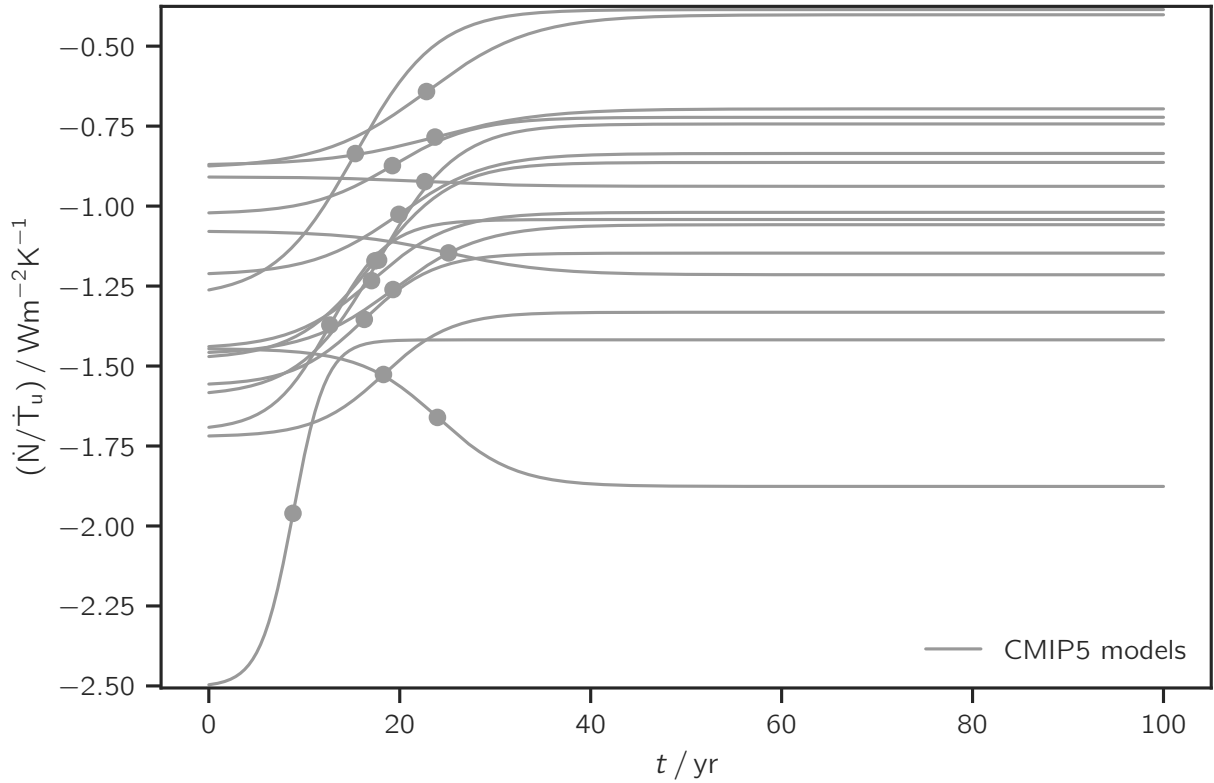
816 **Fig. 3.** Evolution of the slope of the NT -diagram. CMIP5 model behaviour using the fitted pa-
817 rameters presented by Geoffroy et al. (2013a). Dots indicate the time of the sign reversal.
818 Note that three models (CNRM-CM5.1, BNU-ESM and INM-CM4) show a steepening slope
819 instead of flattening. For these models, the fitted ε is lesser than one. 42



820 FIG. 1. Schematic representation of an NT -diagram for constant forcing due to a doubling of the atmospheric
 821 carbon dioxide concentration (F_{2x}). Magenta line represents the relationship between the TOA net radiative
 822 flux change with the surface temperature change if the feedback mechanisms on surface warming were constant
 823 (constant slope). Green line shows the case found in most models, where the slope varies throughout the process.
 824 Given that most models are not run until equilibrium, the evolving slope introduces considerable uncertainty in
 825 the equilibrium climate sensitivity (ECS) estimates



826 FIG. 2. Evolution of the slope of an NT -diagram. Blue solid line, with the average parameters from CMIP5
 827 models obtained by Geoffroy et al. (2013a). Red solid line, with the thermal capacities as calculated by Jiménez-
 828 de-la-Cuesta and Mauritsen (2019). Red dashed line, with C_d as in Jiménez-de-la-Cuesta and Mauritsen (2019).
 829 Red dash-dotted line, with C_u as in Jiménez-de-la-Cuesta and Mauritsen (2019). Dots represent the slope values
 830 when the ratio term \dot{T}_a/\dot{T}_s has the sign reversal. Thin black line is the constant $\lambda = -1.18 \text{ W m}^{-2} \text{ K}^{-1}$.



831 FIG. 3. Evolution of the slope of the NT -diagram. CMIP5 model behaviour using the fitted parameters
 832 presented by Geoffroy et al. (2013a). Dots indicate the time of the sign reversal. Note that three models (CNRM-
 833 CM5.1, BNU-ESM and INM-CM4) show a steepening slope instead of flattening. For these models, the fitted ε
 834 is lesser than one.